Sustainable Food Technology

ROYAL SOCIETY OF CHEMISTRY

PAPER

View Article Online
View Journal | View Issue

Cite this: *Sustainable Food Technol.*, 2026, 4, 2055

Fabrication and characterization of custard apple seed starch/ corn starch bio-nanocomposite films immobilized with chitosan nanoparticles and pomegranate peel powder for extending the shelf life of *Litchi chinensis* fruit

Sachin P. Shinde, * Swapnali S. Bhole, Namita S. Patil, Gurunath V. Mote* and Vikramsinh M. Ingale

The study aimed to develop a bio-nanocomposite packaging film by valorizing agricultural by-products, specifically custard apple seed starch (CaSS), and incorporating varying concentrations of chitosan nanoparticles (ChNPs) with corn starch (CS), carrageenan (CAR), guar gum (GUG), and pomegranate peel powder (PPP). This approach seeks to extend the shelf life of litchi and explore alternative, underutilized resources that can contribute to sustainability and add value to agricultural waste. The composite films form a dense polymer network, enhancing the packaging's attributes. However, the film-forming solution's viscosity decreases with the addition of ChNPs. Further characterization using SEM, FTIR, GC-MS, and XRD revealed improved intermolecular interactions, bioactive compounds, and crystallinity of the films. The addition of ChNPs and PPP significantly reduces moisture content and the water vapour permeability (WVP) rate of the film. The films exhibited an antimicrobial activity against *Pseudomonas fluorescens* and *Botrytis cinerea*. The developed films were tested for their effectiveness in extending the shelf life and maintaining the physicochemical characteristics of litchi. Nevertheless, films composed of CaSS/CAR/GUG without CS/PPP/ChNPs displayed discoloration, color changes, and microbial growth after 2 ± 1 days at 27 ± 2 °C and 65 ± 5% relative humidity (RH). In contrast, CaSS/CAR/GUG/CS/PPP films with 3% ChNPs showed similar changes after 5 ± 1 days, effectively extending the shelf life by an additional 3 ± 1 days, reducing postharvest losses, and increasing value to the fruit industry.

Received 23rd October 2025
Accepted 31st December 2025

DOI: 10.1039/d5fb00721f

rsc.li/susfoodtech

Sustainability spotlight

This research demonstrates a sustainable approach for valorizing agricultural by-products by fabricating bio-nanocomposite packaging films using custard apple seed starch, corn starch, chitosan nanoparticles, and pomegranate peel powder. The study promotes circular economy principles by converting discarded fruit seeds and peels into functional biodegradable materials that replace conventional plastics. The developed films effectively extended the shelf life and preserved the quality of *Litchi chinensis* fruits through improved barrier and antimicrobial properties. By integrating waste reduction, bioresource utilization, and food preservation, this work contributes to sustainable packaging innovations, enhances food security, and aligns with the United Nations' Sustainable Development Goals on responsible production and consumption.

1 Introduction

In the agricultural sector, the fruit and vegetable industry continues to expand rapidly, with fresh litchi (*Litchi chinensis*) emerging as one of the most popular and widely traded commodities in Indian and global markets.[1] The global litchi market was valued at about US $7.02 billion in 2024, and is expected to reach US $11.20 billion by 2033 with a projected CAGR of 5.3% during 2025–2033 (Straits Research Report, Maharashtra). Litchi is an excellent source of vitamins and minerals and is in high demand in local and foreign markets throughout summer due to its delicious, aromatic, nutrient rich aril, and appealing red pericarp.[2] However, harvested fresh litchi is a non-climacteric fruit with a short shelf life of 2–3 days at ambient temperatures due to rapid physiological deterioration, including pericarp browning, discoloration, and enzymatic reactions, leads to substantial postharvest losses ranging from 20% to 30%.[3] Additionally, the disposal of litchi waste represents a significant sustainability concern; large volumes of discarded fruit contribute to food loss and deplete natural

Department of Food Technology, D. Y. Patil Agriculture & Technical University, Talsande, Kolhapur 416112, India. E-mail: gurunathmote@dyp-atu.org; sachinshinde.pgft22@dyp-atu.org

resources such as water, land, and energy. However, when dumped in landfills, decomposing litchi generates methane, a potent greenhouse gas, and can contaminate soil and water systems, disrupting local ecosystems. Thus, reducing fruit wastage is not only essential for economic value but also for environmental management. However, to address these challenges the industry relies on various postharvest techniques which have been employed including modified atmosphere packaging, UV treatment, heat treatment, and chemical preservatives to increase the shelf life and prevent the action of oxidising enzymes like polyphenol oxidase and peroxidase in litchis.[4] However, these techniques are expensive and labour-intensive, and may negatively impact the sensory attributes of fruits.[5] Although chemical agents such as SO_2 fumigation, chlorine-based sanitizers, and synthetic fungicides are used to preserve litchi freshness, they pose notable safety and environmental risks due to potential health risks, residual toxicity, and environmental contamination. Moreover, their routine use leads to soil and water contamination and promotes the development of resistant microbial strains.

To mitigate these challenges, bio-nanocomposite films have garnered significant attention as promising, environmentally friendly packaging alternatives capable of extending the shelf life and preserving the quality of fresh cut fruits.[6–9] Among bio-based polymers, starch-based films, in particular, offer advantages such as edibility, low cost, biodegradability, and excellent barrier properties. However, their high water sensitivity and limited mechanical strength restrict broader application, necessitating thorough evaluation through various experimental techniques.[10] To overcome these limitations and enhance film performance, researchers are increasingly focusing on strategies such as incorporating co-biopolymers, embedding nanoparticles, and integrating antimicrobial agents, thereby creating viable alternatives to petroleum derived packaging materials.[11]

Among these innovations, the incorporation of nanoparticles into biopolymers has emerged as an effective method for improving functional properties due to their nanoscale size, extensive surface area, and strong matrix filler interactions. Additionally, nanoparticles significantly enhance the mechanical, thermal, and barrier properties of polymer films. Recent studies have particularly emphasized biobased nanocomposite packaging materials enriched with naturally occurring antimicrobial compounds and silver nanoparticles to extend the shelf life of fruits.[12–15]

However, starch has gained significant interest as an organic filler because it is inexpensive, biodegradable, easy to process, and readily available. While staple crops such as corn, cassava, rice, wheat, and potatoes are common sources of starch, growing demand for sustainable packaging solutions has encouraged exploration of alternative, non-traditional starch sources. As a result, starch extracted from mango kernels,[16] jackfruit seeds,[17] loquat seeds,[18] and jamun seeds[14] has gained attention as sustainable alternatives to conventional starches. These underutilized sources not only offer potential for developing eco-friendly packaging materials but also contribute to the valorization of agricultural by-products, aligning with circular economy principles.

Accordingly, custard apple (*Annona squamosa*) seed represents another promising raw material source for sustainable packaging. Custard apple is popularly referred to as "sugar apples" or "sitaphal". Industrial processing facilities for custard apples produce a lot of seeds, skins, and seed coatings.[19] However, the inedible portion of the fruit is thrown away as waste or seed waste, and the seeds are underutilized. The left-over custard apple seed contains a variety of beneficial bioactive substances[19–21] and is a good source of minerals like calcium, iron, and sodium together with carbohydrates, protein, and sulphur-containing amino acids like cystine and methionine.[20] Therefore, extracted custard apple seed starch (CaSS) is a promising raw material for sustainable packaging. However, its low amylose content, poor water resistance, and inadequate intermolecular interactions[22–24] result in films produced from CaSS alone exhibiting brittleness, necessitating further modification.

Therefore, the present study integrates CaSS with co-biopolymers such as corn starch (CS), carrageenan (CAR), and guar gum (GUG) for their complementary functional attributes. CS enhances structural strength and reduces brittleness, while CAR and GUG improved flexibility, smoothness, and water resistance.[24] Furthermore, the incorporation of nanoparticles for strengthening biopolymer matrices in bio-nanocomposites has been proposed as a potential solution to the drawbacks of biopolymer-based packaging materials.[25] Adding nanoparticles (NPs) to a continuous biopolymer phase creates three-dimensional networks that improve elasticity, protect against storage instabilities, and improve intermolecular interactions.[26,27] These nanoparticles improve processibility, efficiency, and consumer performance by increasing the rheological, physical, mechanical, and thermal properties.[28] However, they act as reinforcing fillers in the film matrix. As a result, ChNPs distinguish themselves as an effective antimicrobial nanofiller in the organic domain. The previous studies of ChNPs have demonstrated their capacity to improve the functional performance of potato starch,[29] zein,[28,30] and tara gum[31,32] films.

However, packaging materials that incorporate active compounds are more efficient at inhibiting oxidation and microbial growth.[33] Starch molecules are not active against microorganisms and starch films do not possess strong antimicrobial properties. To impart additional bioactivity, waste materials rich in active components, such grape peels and turmeric, have also been used in recent studies as active ingredients in packaging films.[34] To mitigate oxidative degradation and microbial growth, pomegranate peel powder (PPP), a rich source of polyphenols with strong antioxidant and antimicrobial properties, is incorporated as a natural active agent. PPP, derived from fruit-processing waste, supports sustainability goals while contributing to microbial inhibition and oxidative stability in packaging applications.[35,36]

Therefore, the present study aims to develop multifunctional CaSS based bio-nanocomposite films incorporating CS, CAR, GUG, ChNPs, and PPP to extend the shelf life of fresh litchi. Further study focused on exploring alternative, underutilized

resources that can contribute to sustainability and add value to agricultural waste. The films were evaluated for their mechanical, thermal, water vapor barrier, and antimicrobial properties. Moreover, incorporating ChNPs and PPP as an organic nanofiller to functionalize the films would enhance their mechanical, thermal, water vapour barrier, and antimicrobial properties.

Furthermore, fresh litchi (*Litchi chinensis*) was used as a model food system to assess the practical applicability of the developed bio-nanocomposite. Overall, this research contributes to the development of high-performance, bio-nanocomposite biodegradable packaging films derived from agricultural byproducts and developed films used for shelf-life extension of litchi fruit. The bio-nanocomposite films hold significant potential for improving the supply chain, storage, and postharvest management of fresh litchi, reducing supply chain losses, and enhancing sustainability in the fruit industry across local and international markets.

2 Materials and methods

2.1 Raw materials and chemicals

The custard apple seed was procured from M/S. Nutrixia Food, Mumbai, Maharashtra, India. Fresh pomegranates and litchi were obtained from M/S. AB Fruits, a local market located in Kolhapur, Maharashtra, India. Corn starch (Molecular formula: $(C_6H_{10}O_5)_n$, batch number: 2804) was sourced from Indian Fine Chemicals, Bengaluru, Karnataka, India. Chitosan (molecular formula: $(C_6H_{11}NO_4)_n$, molecular weight: 3800–20000 with >75% degree of deacetylation), glycerol, guar gum (Qualigens Fine Chemicals), carrageenan (Grade: Watergel GU 8932), and broth were all procured from Himedia Limited, Mumbai, India. Sodium tripolyphosphate was obtained from Sigma-Aldrich Limited, India.

2.2 Microbial strains

Pseudomonas fluorescens (MTCC-103) and *Botrytis cinerea* (MTCC-2104) were used in this study, both of which were procured from the CSIR–Microbial Type Culture Collection and Gene Bank (MTCC), Institute of Microbial Technology, Chandigarh, Haryana, India.

2.3 Experimental methods

2.3.1 Functionalization of raw materials

2.3.1.1 Isolation of custard apple seed starch (CaSS). Custard apple seeds were processed to isolates CaSS. The seeds were cleaned, dried at 50 °C for 3 h, and then ground into a fine powder. This powder was mixed with a 0.05 M NaOH solution at a 1 : 4 ratio and allowed to react for 7 h. The mixture was then centrifuged at 7000×*g* for 20 min at 4 °C and the precipitate was collected and re-extracted under identical conditions. After the second extraction, the residue was washed with distilled water, neutralised with a 0.1 M HCl solution and filtered through a 75 μm mesh. The mixture was subsequently centrifuged at 5000×*g* for 20 min at 4 °C.[14] The residue was then repeatedly cleaned with distilled water and dried overnight at 45 °C.

2.3.1.2 Preparation of pomegranate peel powder (PPP). The pomegranate peels were first chopped into smaller pieces and then dried for 24 h at 30 °C in a vacuum oven (Labmatrix Manufacturing LLP, Bangalore, India). The dried peels were then ground into a powder using a mixer grinder (Panasonic MX-AC300). The ground pomegranate peel powder (PPP) was further sieved using a sieve shaker (Star Trace Solutions, Chennai; Mesh size: 10) to obtain a uniform particle size of approximately 2 mm.[36] The sieved PPP was then collected and stored in a refrigerator at 4 ± 1 °C until further use.

2.3.1.3 Chitosan nanoparticles (ChNPs). ChNPs were synthesized by the ionotropic gelation technique using chitosan and sodium tripolyphosphate (TPP), following a slightly modified procedure.[37] Chitosan was dissolved in a 1% v/v acetic acid solution and stirred overnight to create a 100 mL chitosan solution (1% w/v). The solution was then centrifuged for 30 min at room temperature at 8603×*g* RCF and the supernatant was gathered.

In parallel, a 40 mL TPP solution (0.4% w/v) was developed and vigorously stirred before being added dropwise to the chitosan supernatant at a rate of 1 mL min^{-1}. The resulting mixture was centrifuged for 30 min at 4 °C and 8603×*g* RCF and the precipitate was collected and frequently washed with deionized water. To achieve a homogeneous suspension, the precipitate was sonicated at 60% amplitude for 5 min and then dried.

The produced ChNPs were analyzed using dynamic light scattering (Malvern Zeta Sizer, Model: NANO-ZS, UK), Fourier transform infrared spectroscopy (Bruker FT-IR TENSOR II, Boston, MA, USA), and X-ray diffraction equipment (Bruker, Germany).

2.3.2 Development of ChNPs employing bio-nanocomposite films integrating CaSS/CAR/GUG/CS and PPP. To prepare the bio-nanocomposite films, 4 g of CaSS was dissolved in 70 mL of distilled water and stirring was continued at 750 rpm for 15 min while heating to 90 °C, followed by cooling while stirring. A CAR solution was made by dissolving 2 g of CAR powder in 200 mL of distilled water at 28 °C for 30 min, and then mixed into the CaSS solution. 0.5 g of GUG was dissolved in 80 mL of 40 °C distilled water and added to the CaSS/CAR solution. After stirring for 30 min at 800 rpm with the addition of 30% glycerol, the CaSS/CAR/GUG film was formed. This solution was heated again to 90 °C for 15 min and stirred continuously for 30 min. 2 g of CS, dissolved in 50 mL of distilled water, was added to create the CaSS/CAR/GUG/CS films, followed by glycerol (30% w/w of polymers) and mixing was continued for 30 min. For the CaSS/CAR/GUG/CS/PPP films, 1 g of PPP was incorporated and stirred for an additional 30 min. Additionally, ChNPs, prepared separately in a 0.2% acetic acid solution at concentrations of 1%, 3%, and 5% weight of polymer, were incorporated into the films by adding 4 g of CaSS to the ChNP dispersion, heating to 90 °C for 15 min and stirring at 750 rpm. The film forming solutions CaSS/CAR/GUG (control), CaSS/CAR/GUG/CS, CaSS/CAR/GUG/CS/PPP, CaSS/CAR/GUG/CS/PPP/ChNP1, CaSS/CAR/GUG/CS/PPP/ChNP3, and CaSS/CAR/GUG/CS/PPP/ChNP5 were combined and evenly

distributed across a 38 × 30 cm diameter Teflon casting plate and dried under IR light for 20 h, and finally vacuum-sealed and stored at 4 ± 1 °C in poly-laminated pouches until use. These films, denoted based on their compositions, were developed to assess their suitability for food packaging applications, focusing on extending shelf life and preserving the quality of perishable products like litchi.

2.4 Characterization techniques

2.4.1 Proximate composition and elemental analysis of CaSS. The proximate composition of the extracted CaSS was determined according to the AOAC method.[38] Moisture content was measured using the oven drying method at 105 °C for 3 h, while ash content was determined by incineration in a muffle furnace at 550 °C for 8 h.[14] Crude protein content was estimated using the Kjeldahl method with a nitrogen to protein conversion factor of 6.25.[39] Fat content was quantified using a Soxhlet extraction apparatus. The amylose content of CaSS was analyzed according to the prescribed procedure.[40] The elemental composition of the CaSS was analyzed using scanning electron microscopy coupled with energy-dispersive X-ray spectroscopy (EDX) at an accelerating voltage of 5 kV. Prior to analysis, the samples were sputter-coated with gold and mounted on aluminum stubs.[41]

2.4.2 Physical, mechanical, and optical properties of films

2.4.2.1 Thickness, moisture content, and film solubility in water. To measure the film thickness, three randomly selected 80 mm × 80 mm test pieces were obtained from each sample to minimize the impact of overhanging mass on micrometer readings. A total of ten test pieces were prepared, and an external digital micrometer with 0.001 mm accuracy (Messmer Instrument Ltd, United Kingdom, Serial No. 100762-01) was employed. The average of five measurements, including the ends and middle from each sample was used to calculate the thickness of the film, following the ISO 534 (International Organization for Standardization) method.[42] Moisture content and water solubility were determined using the reported procedure.[43]

2.4.2.2 Tensile strength. The tensile strength was measured according to American Society for Testing and Materials (ASTM), Method D 882–88. The tensile strength of the films was measured using a Universal Testing Machine (Lloyd Instruments Limited, West Sussex, England). Film samples were cut into rectangular strips measuring 2.54 cm × 15 cm using a precision double blade cutter (Model LB.02/A, Metrotech, S.A., San Sebastian, Spain). A 500 N load cell and an initial grip separation of 50 mm were used, with a crosshead speed of 50 mm min^{-1}, to determine the tensile strength (TS). To calculate TS (in MPa), the maximal force (N) needed to pull the sample apart was divided by the film sample's initial cross-sectional area (m^2). Each film sample was examined in three replicates, and the mean values were calculated and reported.

2.4.2.3 Film colour measurement. The colour parameters of the films, including ΔE (total colour difference), b^* (blueness-yellowness), a^* (greenness-redness), and L^* (lightness), were measured using a Konica Minolta CM-5 spectrophotometer (Serial Number: 1101796) from Konica Minolta Optics, Inc., Japan.

The ΔE values were computed using the following equation:

$$\Delta E = \sqrt{((\Delta L^*)2 + (\Delta a^*)2 + (\Delta b^*)2)}$$

The standard Hunter L^*, a^*, and b^* values for the film samples were established based on the reported study.[42]

2.4.2.4 Opacity. Opacity of the films was determined using a previously reported method.[44] A UV-vis spectrophotometer (LAMBDA 365 UV/vis spectrophotometer) was employed to measure the absorbance at 600 nm. Each film sample, cut into a rectangle measuring 0.7 cm by 1.5 cm, was placed directly into a spectrophotometer test cell. An empty test cell served as the reference.

The opacity (T) of the film was calculated using the formula:

$$T = \mathrm{Abs}_{600}/d$$

where d is the thickness of the film (mm) and Abs600 is the absorbance value at 600 nm. Therefore, higher T values indicate greater opacity and reduced transparency of the films.[45]

2.4.2.5 Water vapor permeability (WVP). The water vapor barrier properties of the film samples were assessed according to ASTM E96/E96M-16 standards. Each sample was used as a lid for jars filled with 30 mL of water, which were then sealed at 23 ± 2 °C and 65 ± 5% RH. Prior to testing, the samples were conditioned to stabilize humidity effects.

To measure the WVP, the jars with sealed samples were weighed before and after a minimum period of 24 h. This process was repeated three times for each sample to ensure accuracy. The WVP, expressed in units of g m^{-2} 24 h^{-1}, was calculated based on the weight changes observed during the test period. This methodology was used to determine the water vapor barrier properties of packaging materials.[17]

2.4.3 Viscosity of film forming solutions (FFSs). A Brookfield DV-II + Pro was used to measure the viscosity of the prepared FFSs. To measure the viscosity of FFSs, the viscometer probe was inserted into a film solution. The findings are presented as mean standard deviation ($n = 3$), despite each reading taken in triplicate.

2.4.4 Scanning electron microscopy (SEM). The morphologies of the films were analyzed utilising 5 kV accelerating voltage scanning electron microscopy (SEM) (Hitachi, Thermo Fisher Scientific, Model: S-3400 N, Noran System 7, Japan) using the reported method.[46] The SEM examination made use of a tungsten filament, and backscattered electrons to examine the surface characteristics of the films. All film samples were firmly attached on aluminium stubs using carbon adhesive tape prior to examination. Subsequently, a thin layer of gold was sputter-coated onto the samples to enhance their conductivity and improve the quality of imaging during SEM observation.

2.4.5 Fourier transform infrared (FTIR) spectroscopy. The FTIR spectra of the developed CaSS and films were obtained using a Bruker FT-IR TENSOR II spectrometer equipped with an attenuated total reflectance (ATR) mode diamond crystal accessory. Spectra were recorded from 4000 to 400 cm^{-1} with a resolution of 4 cm^{-1}. Prior to analysis, a blank open beam background

spectrum was recorded to ensure accuracy. Each spectrum was averaged from 16 images to enhance signal clarity and noise reduction.[41]

2.4.6 Gas chromatography-mass spectrometry (GC-MS) profile. The produced films were subjected to GC-MS analysis using an Agilent Technologies GC system (7890B model), employing two RTx-wax fused silica capillary columns (25 m length, 250 μm diameter, 0.25 μm film thickness) in the Solid Phase Micro Extraction (SPME) GC-MS method. Helium (99.995% purity) was used as the carrier gas at a constant flow rate of 1 mL min^{-1}. The injection temperature was set at 250 °C with a 0 μL injection volume and a split ratio of 0 : 1. Transfer and source temperatures were maintained at 200 °C and 180 °C, respectively. The temperature ramp program included ramps of 5 °C min^{-1} to 110 °C, 3 °C min^{-1} to 150 °C, and 20 °C min^{-1} to 230 °C, with appropriate hold times. Peak retention times, areas (%), heights (%), and mass spectrum fragmentation patterns were utilized for compound identification, cross referenced with the NIST mass spectral library. Relative percentages of components across three concentration levels were calculated by contrasted total areas with base peak areas.[42]

2.4.7 X-ray diffraction (XRD). An X-ray diffraction device was used to obtain XRD patterns of the CaSS and films to determine the degree of crystallinity (Bruker, Germany). Cu Kα radiation ($\lambda = 1.54187$ Å) was used in the diffraction range of 5–600 2θ, with a scanning rate of 70 min^{-1} and a step size of 0.020.[14]

2.4.8 Antimicrobial activity of the film. The efficiency of the ChNP loaded films against *Botrytis cinerea* and *Pseudomonas fluorescens* microorganisms was assessed using the disc diffusion method.[47] In summary, samples measuring 10 mm in diameter were placed onto agar plates after 100 μL of the microbial suspension was poured upon them. The zone of inhibition was evaluated after the plates were incubated for 24 h at 37 °C.

2.4.9 Biodegradability test. To assess the biodegradability of the films, a standardized indoor soil burial test was conducted.[48] Initially, film samples measuring 2 cm × 2 cm were dried in an oven at 60 °C for 24 h to achieve consistent dry weights (W_1). These samples were then placed in cups with aluminum mesh, buried 4 cm deep in soil, and subjected to daily watering to maintain soil moisture under natural conditions. After a 20 day burial period, the films were carefully excavated from the soil, cleaned to remove any adhering soil, and dried again at 60 °C for 24 h to obtain final dry weights (W_2). The percentage weight reduction was calculated using the formula:

$$\text{Weight reduction (\%)} = W_1 - W_2/W_1 \times 100$$

2.5 Selection, storage, and packaging of the selected sample (litchi)

2.5.1 Selection of the selected sample (litchi). The litchi sample selection process began with the procurement of fresh litchi from AB Fruits, a local market located in Kolhapur, Maharashtra, India. To maintain optimal freshness and minimize postharvest effects, the litchi was delivered to the laboratory within 6 h of harvesting. Upon arrival, rigorous inspection and sorting procedures were conducted to ensure uniformity and uphold quality standards. Each litchi was carefully hand sorted to maintain its integrity, consistent colour, and size, while any litchi showing signs of infection, disease, decay, or damage was promptly removed.

2.5.2 Storage and packaging of litchi. In the experimental trials, freshly sorted litchi was immediately packed and stored under controlled conditions in the temperature range of 27 ± 2 °C with 65 ± 5% RH for a duration of 5 days. Each packet contained 100 g of litchi and was packed in developed films measuring 20 × 15 cm pouch dimension, and sealed with a pneumatic sealing machine from Sunray Industries. The final packs were organized with each treatment comprising five packets. The six treatments evaluated were CaSS/CAR/GUG, CaSS/CAR/GUG/CS, CaSS/CAR/GUG/CS/PPP, CaSS/CAR/GUG/CS/PPP/ChNP1, CaSS/CAR/GUG/CS/PPP/ChNP3, and CaSS/CAR/GUG/CS/PPP/ChNP5. Throughout the storage period at 27 ± 2 °C with 65 ± 5% RH, physicochemical and sensory evaluations were conducted on 0, 1, 2, 3, 4, and 5 days. Triplicate analyses were performed for each evaluation to ensure consistency and reliability of the results.

2.6 Qualitative measurements for the shelf- life evaluation of litchi

2.6.1 Sensory assessment. The sensory assessment involved a panel of 10 semi-trained individuals, including academic members and research participants from DYP-ATU, Talsande, India, aged between 26 and 55 years. Using a 9 point hedonic scale where 1 represented "extreme dislike" and 9 indicated "extreme liking",[49] the panel evaluated litchi samples under controlled conditions of 27 ± 2 °C with 65 ± 5% RH. Various sensory attributes such as freshness, appearance, colour, aroma, discoloration, texture, defects, and overall acceptability were assessed. To maintain objectivity, samples were evaluated anonymously using assigned codes. The assessment was conducted at room temperature, and the overall acceptability was determined by averaging scores across all attributes. The end of shelf life was identified as the point where the average score reached 5 on the hedonic scale; scores below 5 were considered undesirable, aligning with criteria established.[50]

2.6.2 Moisture content. To determine the moisture content of litchi, fresh samples were finely chopped and 5–10 g were placed in a pre-weighed, dry Petri dish. The dish with litchi was dried in an oven at 130 ± 5 °C for 2 h, cooled within a desiccator, and reweighed. Moisture content (%) was calculated using:

$$\text{Litchi moisture content (\%)} = (W_1 - W_2) \times 100/(W_1 - W)$$

Here, W_1 is the dish's initial weight (in g) including the litchi pieces prior to drying, W_2 is the dish's weight (in g) containing the dried litchi pieces following drying, and W is the weight (in g) of the empty dish. This method ensured precise measurement of moisture, critical for assessing litchi quality and shelf life.[51]

2.6.3 pH value measurement. During storage, litchi pH was measured using a LAQUA pH 1500-meter, model A82A0059, offering precision up to 0.001%. Litchi samples (3 g each) were mashed and dissolved in 10 mL of distilled water for analysis. Three measurements were conducted for each treatment to ensure accuracy.[52]

2.6.4 Firmness. Textural parameters during storage were assessed by puncturing each litchi sample three times at 4 mm intervals on the equatorial region using a texture analyzer (TA.HD plus, Stable Micro Systems, UK) equipped with a 5 kg load cell and a 2 mm diameter stainless steel probe. The texture analyzer settings included a pre-test speed of 2 mm s^{-1}, a test speed of 1 mm s^{-1}, and a post-test speed of 2 mm s^{-1}. Peel firmness (N) was determined as the maximum force required to break the peel, recorded from the equatorial region for consistency.[53] Nine readings per parameter per treatment were averaged for analysis and reported.

2.6.5 Total soluble solid (TSS) content. To determine the TSS of each treated litchi sample, 5 g of litchi were crushed using a mortar and pestle. The resulting mixture was then filtered using muslin cloth, and approximately 1 mL of the filtrate was transferred to the prism of a refractometer for measurement. The TSS content was measured using a digital refractometer (Model Number: HI96801, Hanna Instruments), with values expressed in degrees Brix (°Brix) serving as an indication of the soluble solids present.[54]

2.6.6 Titratable acidity (TA). The procedure used to estimate titratable acidity (TA) involved homogenizing 10 g of litchi pulp in 100 mL of distilled water and filtering the mixture. A faint pink tint developed due to the presence of 1% phenolphthalein, indicating that the filtrate had reached the end point, which was titrated with 0.1 N NaOH. The TA results are given as a percentage (%).[52]

$$\%\ \text{Acidity} = \text{mL NaOH} \times 0.1\text{N NaOH} \times 0.064 \times 100/\text{volume of sample (mL)}$$

2.6.7 TSS : TA ratio. The TSS : TA ratio is a critical parameter for assessing fruit ripeness and its impact on taste and overall quality perceived by consumers. After measuring both total soluble solids (TSSs) and titratable acidity (TA), the TSS : TA ratio was calculated by dividing the TSS value by the TA value. This ratio offers valuable insight into the balance between sweetness (indicated by TSS) and acidity (indicated by TA) in the fruit, aiding in the evaluation of its optimal ripeness level and sensory appeal.[54]

2.6.8 Percent of fresh litchis. To assess the percentage of fresh litchi, visual evaluations were conducted on all litchis from each treatment at each sampling point. The assessment included observations of colour, texture, wilting, appearance, microbiological growth, and other relevant variables.[42] The percentage of fresh litchi was calculated using the formula:

$$\text{Fresh litchi (\%)} = (\text{number of fresh litchis on the day of examination} \times 100)/\text{total number of litchis}$$

2.6.9 Colour assessment. A Konica Minolta CM-5 spectrophotometer (Serial Number: 1101796) measured the colour of all treated samples at three positions on the equatorial region. Hunter parameters assessed were lightness (L^*), redness-greenness (a^*), and yellowness-blueness (b^*). The total colour difference (ΔE) was computed using:

$$\Delta E = \sqrt{((\Delta L^*)2 + (\Delta a^*)2 + (\Delta b^*)2)}$$

Standard Hunter L^*, a^*, and b^* values for the litchi samples were established following a previously reported method.[42] ΔE indicates the deviation in colour values between the final sample and showing the colour change of the samples over time.

2.6.10 Weight loss percentage. To determine the litchi weight loss percentage during storage, initial weights (W_i) were recorded. Over 0 to 5 days, final weights (W_f) of selected litchi samples (three per test) were measured using an analytical balance.[55] Weight loss (%) was calculated as:

$$\text{Weight loss (\%)} = (W_i - W_f)/(W_i) \times 100$$

2.7 Statistical analysis

The physicochemical, mechanical, microbial, and sensory data obtained from all treated samples were analyzed using analysis of variance (ANOVA) in SPSS software (version 20.0; IBM Corp., Armonk, NY, USA). Post hoc tests (Duncan's test), one-sample *t*-tests, and one-way ANOVA were applied to evaluate variations in litchi sample quality. All statistical analyses were conducted at a 95% confidence interval, with significance set at $p < 0.05$. The results are presented as mean ± standard deviation.

3 Results and discussion

3.1 Characterization of raw materials

3.1.1 CaSS. To maintain their vibrancy and physiological function, chemical composition of CaSS is important for studies. The moisture, ash, fat, and protein contents in CaSS play significant roles in determining the final properties of the films. These components interact with the starch matrix and influence key film characteristics like mechanical strength, flexibility, barrier properties, and stability.

The CaSS exhibited a moisture content of 8.79 ± 0.05%, ash content of 1.38 ± 0.04%, fat content of 0.97 ± 0.04%, and protein content of 0.81 ± 0.03% on a dry weight basis. The amylose content of CaSS was 17.23%, which falls within the reported range for normal starches (15–30%).[56] Moisture content plays a critical role in the film forming properties of starch. An increase in moisture content leads to a reduction in the structural integrity of CaSS, while also influencing its pasting behavior. Additionally, molecular weight dispersion increased and chain length distribution varied with decreasing moisture content.[57] Therefore, moisture content and chemical composition were systematically analyzed.

The FTIR spectrum of CaSS (Fig. SI.1) displayed characteristic absorption bands typical of CaSS. A broad band at 3293 cm^{-1} corresponds to O–H stretching vibrations, indicating extensive intermolecular hydrogen bonding within the starch structure. The absorption peaks observed at 2923 and 2853 cm^{-1} are attributed to C–H stretching vibrations of aliphatic $-CH_2$ and $-CH_3$ groups. The band near 1648 cm^{-1} is associated with H–O–H bending vibrations of absorbed or bound water in the starch granules. Prominent peaks at 1156, 1078, and 1026 cm^{-1} are assigned to C–O–C and C–O stretching vibrations of glycosidic linkages and the glucose ring structure, confirming the polysaccharides in CaSS. Additional absorption bands below 1000 cm^{-1} correspond to skeletal vibrations of the pyranose ring. Overall, the FTIR profile confirms the structural integrity of CaSS, with the presence of dominant alcohol, alkane, and alkene functional groups, consistent with native starch materials.

The X-ray diffraction (XRD) pattern of CaSS (Fig. SI.2) was recorded using Cu Kα radiation ($\lambda = 1.5406$ Å) over a 2θ range of 5°–90°, revealing distinct diffraction peaks that indicate the semi crystalline nature of starch. Prominent reflections were observed at 2θ values of approximately 28.35°, 31.18°, 32.02°, 32.32°, 34.86°, 35.12°, and 46.38°, with the most intense peak occurring at 46.38°, corresponding to a *d*-spacing of 1.96 Å. Additional peaks at higher angles (57.93°, 63.93°, 70.29°, and 75.98°) further confirm the presence of ordered crystalline domains within the starch matrix. The diffraction pattern reflects the characteristic crystalline arrangement of starch granules, arising from the ordered packing of amylopectin double helices interspersed with amorphous regions. The coexistence of sharp crystalline peaks and a broad background suggest partial disruption of crystalline order, consistent with modified or processed starch systems. Overall, the XRD results confirm that CaSS retains a semi-crystalline structure, which is crucial for its functional properties such as film formation and mechanical stability.

The elemental distribution analysis (EDX) was conducted, which enabled the identification of all the major and trace elements and ascertained whether the structures observed contained distinct chemical compounds in CaSS. The elemental analyses of the CaSS performed by EDX are displayed in Fig. 1A. EDX analysis indicated that the structure of starch was composed of carbon and oxygen with atomic percentages. The three elements carbon (C), hydrogen (H), and oxygen (O) should be present as starch is made up of glucose units; nevertheless, only C and O are observable; H cannot be differentiated since hydrogen only consists of valence electrons rather than core electrons. Furthermore, it would be difficult to differentiate the signals generated by H 1s valence electrons because this would overlap with signals from other valence electrons.[58] According to an EDX examination, starch's structure was mostly made up of carbon and oxygen in various atomic percentages. EDX was used to determine the elemental composition of CaSS and confirm its purity by detecting mainly carbon and oxygen with minimal inorganic impurities. The measured starch's atomic percentages of C and O revealed an elemental signature that is distinctive to starch. The atomic percentages of C and O in the quantitative results of the elemental analysis of starch are 62.73% and 36.31%, respectively. Furthermore, a sodium (Na) 0.96% was noted. The EDX results revealed the C and O are the major elements in the CaSS.

3.1.2 ChNPs. Chitosan (Ch) with positively charged amino groups engages in intra or intermolecular ionic interactions with the negatively charged tripolyphosphate (TPP) ions during the ionotropic gelation process to produce ionically cross-linked chitosan nanoparticles. Fig. 1B and C display the ChNP particle size and zeta potential. The zeta potential of 9.77 ± 0.12 mV and average particle size of 178.43 ± 4.11 nm are in accordance with the published studies.[59–61] Previous research has examined the impact of Ch-TPP concentration on particle size.[62] Moreover, an increase in the amount of TPP that is negatively charged resulted in a decrease in zeta potential.[63] The chitosan and Ch-TPP nanoparticle containing film forming solutions were dried to produce flexible, transparent, and surface-smooth films.[59]

Fig. 1D displays the FTIR spectra of the ChNPs (blue spectrum) and chitosan (red spectrum). The chemical compatibility was validated by FTIR spectra, which preserved the integrity of the principal peaks and demonstrated the lack of chemical conflict. Ch specifically shows distinct peaks at 3354 cm^{-1} (–OH stretching), 2874 cm^{-1} (–CH stretching), 1647 cm^{-1} (amide I), 1565 cm^{-1} (amide II), 1375 cm^{-1} (CH_3 symmetrical stretching), 1150 cm^{-1} and 897 cm^{-1} (chitosan's saccharide structure), and 1025 cm^{-1} (C–O–C asymmetric stretching).[37,64]

Additionally, one absorption peak was present in both samples at 3775 cm^{-1}, which was explained by –OH stretching vibrations.[65] The amide I and II peaks in the ChNPs are displaced with higher peak intensities from 1573 cm^{-1} to 1505 cm^{-1}, demonstrating the electrostatic interactions between the phosphate groups of TPP and the amide groups of Ch. The ChNPs reveal an additional peak at 1085 cm^{-1}, which represents the P–O stretching.[66] The improved hydrogen bonding interactions between Ch and TPP are demonstrated by the widened –OH stretching at nearly 2742 cm^{-1} in the ChNPs.

The XRD patterns of Ch and ChNPs are displayed in Fig. 1E. The XRD pattern of Ch exhibited four distinct crystalline peaks at 2θ values of approximately 20°, 29°, 36°, and 48°, corresponding to crystal planes I, II, III, and IV with interplanar spacings of 1.75, 1.85, 2.57, and 10.99 Å, respectively.[67,68] Additionally, the Ch peaks expanded due to the ionic gelation process and decreasing strength of the peak, resulting in the creation of two diffraction peaks in the ChNPs at 2θ values of approximately 23° and 27°. A decrease in the crystalline structure of Ch led to the broadening of diffraction peaks, indicating interactions between TPP and the Ch chains.[28] The diffraction peaks of ChNPs showed a reduced intensity, which indicated that their natural state is amorphous. The purity of ChNPs was demonstrated by thr absence of additional diffraction peaks in their XRD patterns, which corresponded to substances.[69] The improved compatibility and faster rates of dissolution in the polymer matrix provided by the larger surface area of the nanoparticles might be responsible for the decreased crystallinity, which was consistent with the earlier reports.[14]

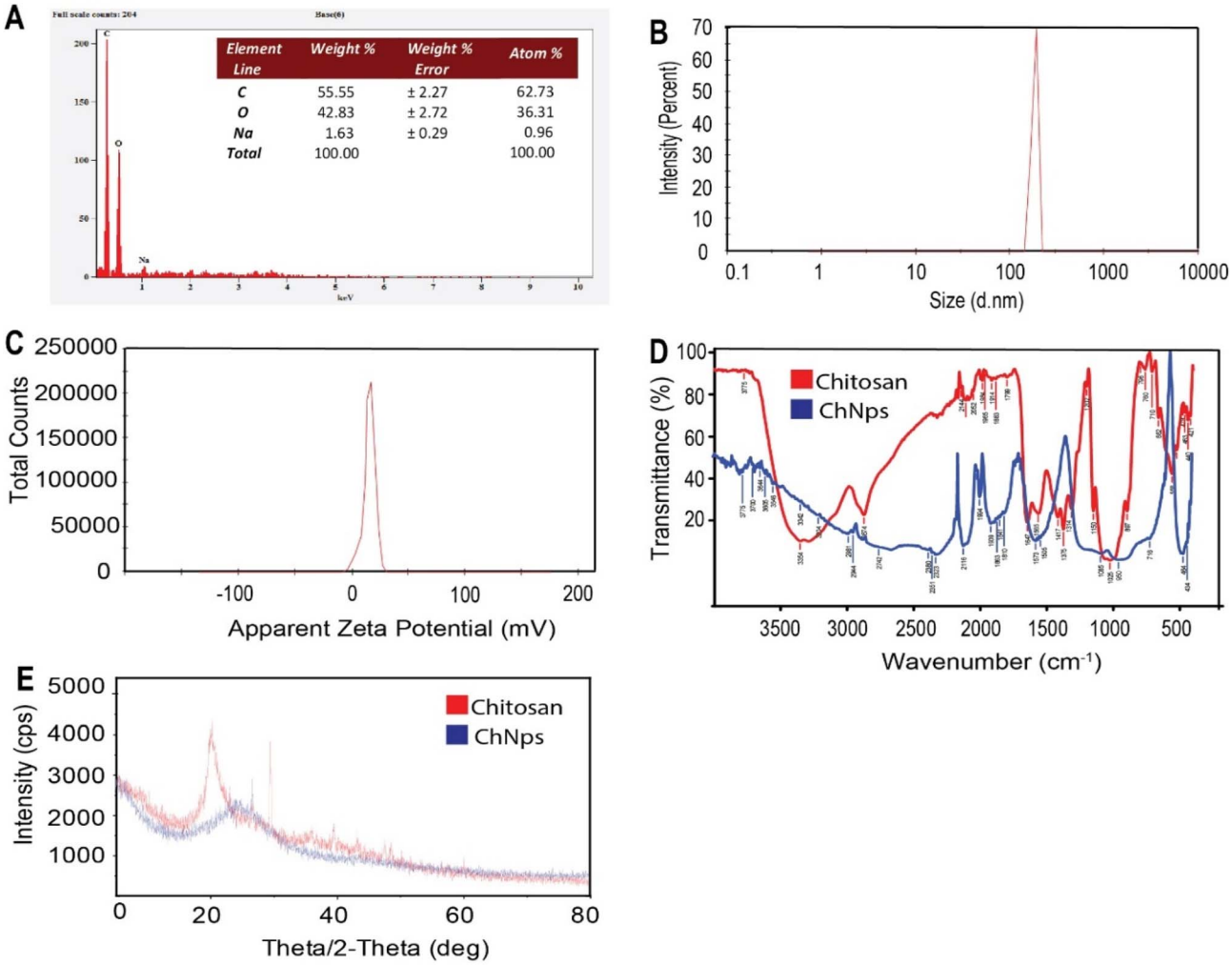

Fig. 1 (A) EDX micrograph of the custard apple seed starch (CaSS); (B) size distribution; (C) apparent zeta potential distribution; (D) FTIR spectra, and (E) XRD diffractogram of chitosan (Ch) and chitosan nanoparticles (ChNPs).

3.2 Characterization of film solutions and films

The following are properties of the developed films that were analyzed to determine the impact of the films.

3.2.1 Physical and optical properties

3.2.1.1 Thickness, moisture content, and film solubility in water. The films thickness, moisture content, and water solubility are shown in Table 1. The measured thicknesses of the CaSS/CAR/GUG, CaSS/CAR/GUG/CS, and CaSS/CAR/GUG/CS/PPP films were 142.10 ± 1.91 μm, 146.30 ± 0.82 μm, and 150.50 ± 1.17 μm, respectively. It is noteworthy that the thickness increased to 155.20 ± 0.91 μm, 160.40 ± 1.34 μm, and 166.40 ± 2.87 μm at concentrations of 1, 3, and 5% respectively, upon the incorporation of ChNPs. Despite the ChNP and PPP concentration of these matrices added within the film, statistically no change was observed in the thickness values of the films ($p < 0.05$). This increasing trend indicates an incrrease in polymer density within the matrix, likely due to the hydrolysis of starch molecules in the ChNP acetic acid dispersion. Furthermore, the thickness of the films is directly influenced by the type of incorporated nanoparticles, the interactions between the nanoparticles, the polymer matrix, and the film forming method.[70] A comparable increase in thickness was noted in films containing starch[71] and on NP incorporation in films.[72]

The moisture content (MC) of the films decreased significantly with the addition of ChNPs and PPP, decreasing from 27.15 ± 0.015 (CaSS/CAR/GUG) to 18.26 ± 0.063% (CaSS/CAR/GUG/CS/PPP/ChNP5). As ChNPs increased, the moisture content of the films reduced considerably ($p < 0.05$) compared to the CaSS/CAR/GUG film. This may be because the PPP and ChNPs were included, which might have an impact on a film's ability to hold onto water.

The water solubility (WS) of the materials employed to produce films is an important factor when adopting a film for a certain application. In numerous situations such as the encapsulation of food, solubility is a desired attribute. Solubility is adverse when it comes to the water resistance and integrity needed for packing meals with high moisture levels. In general, the type of compounds, their quantities, and their intrinsic hydrophilicity and hydrophobicity indices determine how additives affect the solubility of films. However, hydrophilic

Table 1 Comparison of thickness, moisture content, solubility in water, tensile strength, opacity, and water vapor permeability of films. The results are expressed as the mean of three different trials, with statistical significance ($p < 0.05$) and standard deviation determined according to one sample '*T*' test

	CaSS/CAR/GUG	CaSS/CAR/GUG/CS	CaSS/CAR/GUG/CS/PPP	CaSS/CAR/GUG/CS/PPP/ChNP1	CaSS/CAR/GUG/CS/PPP/ChNP3	CaSS/CAR/GUG/CS/PPP/ChNP5
Thickness (μm)	142.10 ± 1.91	146.30 ± 0.82	150.50 ± 1.17	155.20 ± 0.91	160.40 ± 1.34	166.40 ± 2.87
Moisture content (%)	27.15 ± 0.15	25.42 ± 1.10	22.83 ± 0.23	21.06 ± 0.25	19.76 ± 0.30	18.26 ± 0.06
Water solubility (%)	65.40 ± 0.51	69.05 ± 0.07	74.72 ± 0.54	75.95 ± 0.12	75.33 ± 0.36	74.22 ± 0.17
Tensile strength (MPa)	6.43 ± 0.25	9.13 ± 0.16	10.44 ± 0.31	13.54 ± 0.44	16.61 ± 0.22	18.82 ± 0.27
Opacity (*T*)	8.48 ± 0.003	5.51 ± 0.012	4.84 ± 0.003	9.71 ± 0.004	9.41 ± 0.001	9.55 ± 0.003
WVTR (g m^{-2} 24 h^{-1})	11.64 ± 0.29	10.80 ± 0.22	9.57 ± 0.06	8.54 ± 0.432	7.45 ± 0.071	6.72 ± 0.220

compounds are expected to increase a film's solubility while hydrophobic compounds are expected to reduce solubility.[56]

However, there was an increasing trend observed in the WS. According to Table 1, the CaSS based films with incorporation of PPP and ChNPs produced an increase in WS from 65.40 ± 0.51 to 75.95 ± 0.12%, which suggests that the composite film matrix has more hydroxyl groups and is hydrophilic in nature. Furthermore, adding 1% ChNPs enabled the highest WS of 75.95 ± 0.12%, which is explained by the starch molecules that had been hydrolysed making the films more soluble. However, when the concentration of ChNPs was increased to 3 and 5%, the WS was slightly reduced. As a result of the increasing molecular interactions between ChNPs and biopolymers (CaSS/CAR/GUG), water molecules may be restricted from diffusing substantially, which would reduce the solubility of the films. However, for edible films, a moderate to high water solubility could be advantageous so that the substance can be quickly removed from the food surface before eating.[73]

3.2.1.2 Tensile strength. The mechanical properties of films were assessed by determining their tensile strength (TS), which provides an important indicator of their strength. Table 1 shows the effect of ChNP concentrations on the mechanical properties of film samples. When the concentration of ChNPs was increased from 1% to 5%, there was a change in TS, which was caused by an increase in ChNP content in the films ($p < 0.05$). The TS of the CaSS/CAR/GUG films was 6.43 ± 0.25 MPa. However, when CS was combined with CaSS/CAR/GUG, the TS increased to 9.13 ± 0.16 MPa. In the same way, on incorporating PPP into CaSS/CAR/GUG/CS the TS increased up to 62%. The higher TS indicates that polymer intermolecular interactions are creating a stronger network within the composite film matrix. TS improvement is mainly due to strong electrostatic and hydrogen bonding between ChNPs and the film matrix. ChNPs primarily interact with carrageenan through electrostatic attraction, while simultaneously forming hydrogen bonds with starch and guar gum, leading to a denser and stronger composite network. However, increasing 1% ChNPs enables the TS increase to 13.54 ± 0.44 MPa, indicating that ChNPs have become important in the CaSS/CAR/GUG/CS network. This structure was consistent with the hydrolysed starch films[74] and chia mucilage films[75] that were integrated into starch nanocrystals. With a further increase in ChNP content from 3 to 5%, the TS increased to 16.61 ± 0.22 MPa and 18.82 ± 0.27 MPa, respectively. This suggests that ChNPs are uniformly dispersed and reinforce the CaSS/CAR/GUG/CS matrix.

3.2.1.3 Film colour. The colour parameters L^*, a^*, and b^* as well as the overall colour difference (ΔE) values for films are displayed in Fig. SI.3. There was no significant difference ($p < 0.05$) found in any of the films for L^* values. Although the films with ChNPs appeared darker, starch films containing ChNPs generally had lower L^* values. When ChNP concentrations climbed from 1 to 5% (v/v), there were no discernible alterations in L^* values, but there were substantial changes ($p < 0.05$) in b^* values across the same concentration range. The addition of ChNPs caused the emulsified starch with carrageenan films to become opaquer, which is consistent with previous studies.[56] This impact is most likely caused by light scattering in the lipid droplets increasing diffuse reflectance, which reduces both the intensity of light scattering and the whiteness index of the film. The CaSS/CAR/GUG films, the nanocomposite films, revealed a higher total colour difference (ΔE). In overall, the addition of PPP and ChNPs decreased the colour intensities (Fig. SI.3).

3.2.1.4 Opacity. Film opacity is a desirable characteristic in packaging materials, as it protects food from oxidative deterioration induced by visible and ultraviolet radiation. Table 1 displays the opacity of films based on including starch, ChNPs and PPP. The addition of PPP and ChNPs reduced the transparency of the CaSS films, and these results were consistent with previous reports.[76] Whenever chitosan films incorporating ChNPs were compared to other films, their opacity values declined. Additionally, a reduction in film transparency following the incorporation of antioxidants in chitosan based films containing pomegranate rind extract has also been reported.[44]

3.2.1.5 Water vapor permeability (WVP). Table 1 displays the WVP of the films based on CaSS and ChNPs. The CaSS/CAR/GUG films showed the highest WVP of 11.64 ± 0.29 g m^{-2} 24 h^{-1}. However, the composite CaSS/CAR/GUG/CS films showed a decrease in WVP of 10.80 ± 0.22 g m^{-2} 24 h^{-1}. This improvement can be attributed to enhanced intermolecular hydrogen bonding within the polymer matrix, which reduces the availability of free hydroxyl groups necessary for water vapour transport ($p < 0.05$). Stated differently, the tightly packed CaSS molecules, resulting from the compact network formed by ChNPs and PPP chains, hindered water vapour diffusion through the film matrix. Moreover, the uniform distribution of

ChNPs throughout the CaSS/CAR/GUG/CS matrix, which created a long pathway for water vapour transmission, further supports this observation.[77] Furthermore, the interactions between the biopolymers and ChNPs restricted the mobility of water molecules, thereby enhancing the vapour barrier properties of the film matrix.[78] The observed trend is also attributed to the increased surface hydrophobicity of the nanocomposites. Notably, films containing 5% ChNPs exhibited a 42% reduction in WVP compared to the CaSS/CAR/GUG composite films, which is considerably higher than the 18% reduction reported for zein films loaded with chitosan nanoparticles.[28]

3.2.2 Rheological behaviour of film forming solutions (FFSs). Rheological characterization is used to elucidate the relationship between component interactions, polymer structure, and the mechanical behavior of the films.[79] The FFS viscosity is illustrated in Fig. SI.4. CaSS/CAR/GUG exhibited the lowest viscosity (3216 cP) amongst all the FFSs, while CaSS/CAR/GUG/CS/PPP/ChNP5 showed the highest viscosity (5802 cP). Curiously, compared to the CaSS/CAR/GUG blend solutions, the viscosity values increased with the incorporation of 1, 3 and 5% ChNPs, indicating improved hydrogen bonding interactions between polymer chains and ChNPs. However, this increase might be due to CaSS molecule hydrolysis in the acetic acid dispersions of ChNPs. The typical length of the starch chain decreased during the process of acid hydrolysis.[80] A similar viscosity increase was demonstrated substantially while cellulose nanocrystals were incorporated into the cassia gum matrix.[81]

3.2.3 Scanning electron microscopy (SEM). SEM provides high-resolution images at higher magnifications, while also allowing observation of larger sample areas at lower magnifications. The effect of PPP and ChNPs on the film's morphology was evaluated using SEM analysis. Fig. 2 shows the obtained surface micrographs of the nanocomposite films loaded with ChNPs, CaSS, and PPP at the original 20.0 μm magnification. The SEM images (Fig. 2A and B) show the CaSS/CAR/GUG and CaSS/CAR/GUG/CS film's non-uniform microstructure which may be due to the starch molecule's gelatinization. However, potato starch-based films showed to similar microstructures.[82]

The marked surface differences between the CaSS/CAR/GUG/CS and CaSS/CAR/GUG/CS/PPP films indicate improved polymer compatibility and interactions. Similar surface morphology changes have been reported for composite films prepared from tamarind seed starch/gelatine[14] and gelatine/gum tragacanth[83] films. Despite the ChNP agglomeration in the polymer matrix, the incorporation of ChNPs produced surfaces with rough, fiber-like features. Nevertheless, compared to CaSS/CAR/GUG films, incorporating 1, 3, and 5% ChNPs and PPP produced spherical-shaped particles, which indicates enhanced crystallinity and improved mechanical and barrier properties (Table 1).

While the crystallinity of the particles increased, it is noteable that the film's surface became smoother and more compact. Agglomeration of the differently sized particles was observed, with their dispersion occurring at random throughout the substrate. For the chitosan nanoparticle loaded fish gelatine[37] and starch[29] films, similar morphological properties were observed. It seems that larger concentrations of nanoparticles disrupt interactions between chains and generate weak spots in the network of the polymer, which may have an impact on overall properties of the film.

3.2.4 Fourier transform infrared (FTIR) spectroscopy. The FTIR analysis of the interactions between CaSS, CAR, GUG, CS, PPP, and ChNPs is shown in Fig. 3. Several absorption peaks were found that were associated with starch-based films, and significant variations in peak intensities occurred among the film samples.

The primary absorption band observed in CaSS/CAR/GUG films, spanning from 3700–3000 cm^{-1} to 1500–1000 cm^{-1}, is the distinctive O–H and N–H stretching vibration linked to free, inter, and intramolecular hydroxyl groups.[31] The C–H, C–N, C–C, and C–O stretching vibrations are represented by the peaks of absorption located at nearly 2900 to 2800 cm^{-1}, 2324 cm^{-1}, 2114 cm^{-1}, and 1912 cm^{-1}, respectively. The C–O bond's vibrational modes within the pyranose ring are represented by the peak located at around 1153 cm^{-1}.[84] Additionally, it is speculated that the ordered structure and crystallinity of starch molecules are responsible for the strong peaks between 1108 and 1224 cm^{-1}.[85] Similar absorption peaks were observed in the films using CaSS/CAR/GUG/CS/PPP and ChNPs.

There were notable alterations in the –OH stretching vibrations, with a large shift to a larger wavenumber and slight decrease in intensities of the peak within the nanocomposite films. This suggests that CAR, GUG, CS, PPP, and ChNPs formed hydrogen bonding connections with the free hydroxyl groups present in CaSS. The fish gelatine films with ChNPs were found to have similar results.[37] Due to interactions with CAR/GUG/CS/PPP chains, the sharp peak that was observed, which was identified at 2114 and 2324 cm^{-1} in the CaSS/CAR/GUG/CS/PPP films with ChNPs 1 and 3%, widened in the bio-nanocomposite films, indicating a decline in the starch granule's degree of structure.[86]

3.2.5 GC-MS profile. Headspace GC-MS was employed to analyze the developed bio-nanocomposite film to identify the volatile compounds responsible for the activity of the matrix solution. Despite their low concentrations, bioactive compounds from the matrix formulation were detected in the GC-MS profile of the bio-nanocomposite films. Headspace GC-MS was used to examine key compounds, and their relative abundances in the films were determined based on area percentages.

O-Cymene, caryophyllene, γ-terpinene, β-pinene, α-pinene, camphene, *trans*-β-ocimene, and β-bisabolene were among the compounds found due to incorporated PPP and ChNPs 1 to 5% in the films. Furthermore, the previous study showed that custard apple seeds contain volatile substances like β-caryophyllene, α-pinene, β-pinene, camphene, spathulenol, germacrene, myrcene, annonacin, and molvizarin. It also described the medical benefits of bioactive compounds found in custard apple seeds, indicating that these compounds are primarily responsible for the antimicrobial, insecticidal, anti-inflammatory, and anticancer properties.[20] Fig. SI.5 presents the results of the GC-MS examination of the different compounds detected in the CaSS/CAR/GUG, CaSS/CAR/GUG/CS, CaSS/CAR/GUG/CS/PPP, CaSS/CAR/GUG/CS/PPP/ChNP1, CaSS/

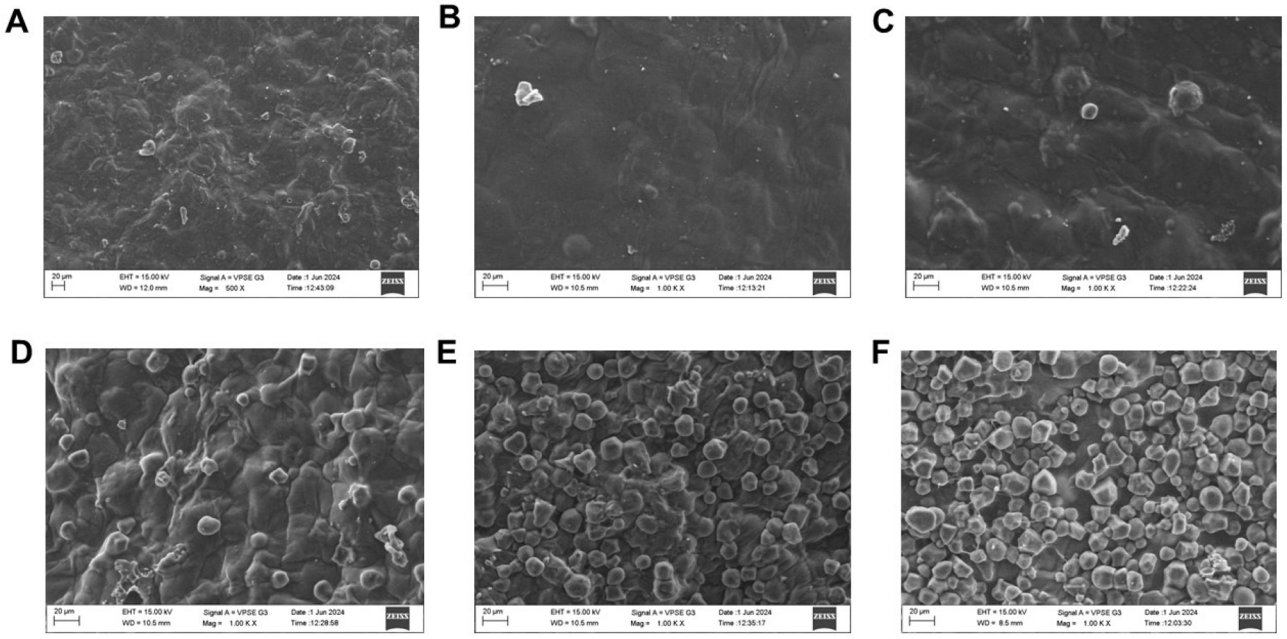

Fig. 2 SEM micrographs of (A) CaSS/CAR/GUG; (B) CaSS/CAR/GUG/CS; (C) CaSS/CAR/GUG/CS/PPP; (D) CaSS/CAR/GUG/CS/PPP/ChNP1; (E) CaSS/CAR/GUG/CS/PPP/ChNP3; and (F) CaSS/CAR/GUG/CS/PPP/ChNP5 films.

CAR/GUG/CS/PPP/ChNP3, and CaSS/CAR/GUG/CS/PPP/ChNP5 films. Table SI.1–6 summarise the bioactive compounds that have been identified. Consequently, the existence of these substances demonstrates the film's antimicrobial properties, which are identical to those of the matrix solution.

3.2.6 X-ray diffraction (XRD). XRD analysis was used to examine the alterations in the crystalline structures of the CaSS, CAR, GUG, CS, PPP, and ChNP loaded nanocomposite films which are demonstrated in Fig. 4 and SI.6.

The CaSS/CAR/GUG films showed a single substantial diffraction peak, which corresponded to the conventional A-starch pattern, at a 2θ value of 22°.[16] Nevertheless, the inclusion of CS resulted in a decrease in the peak intensity at a 2θ value of 21°, indicating the tightly bound biopolymer networks within the composite film matrix. Furthermore, the diffraction peak at approximately 19° of 2θ showed increased intensity and became considerably broader following the addition of PPP.

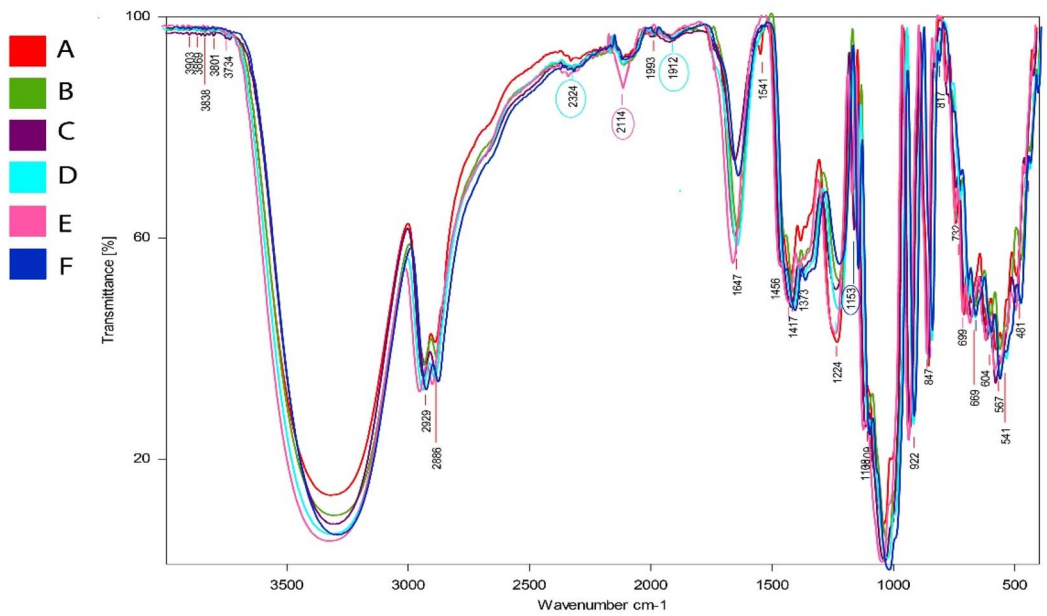

Fig. 3 FTIR transmittance mode spectra of (A) CaSS/CAR/GUG; (B) CaSS/CAR/GUG/CS; (C) CaSS/CAR/GUG/CS/PPP; (D) CaSS/CAR/GUG/CS/PPP/ChNP1; (E) CaSS/CAR/GUG/CS/PPP/ChNP3; and (F) CaSS/CAR/GUG/CS/PPP/ChNP5 films.

Moreover, the diffraction peak at a 2θ value of 20° was further expanded and intensified with the addition of ChNPs. Perhaps the hydrolysis of amorphous areas in the starch granules and the increased crystallinity in the ChNP loaded films as a result of interfacial interactions are responsible for the observed improvement.[82]

3.2.7 Antimicrobial activity of films. Table 2 and SI.7 depict the antimicrobial activity of the produced film forming solutions against *Pseudomonas fluorescens* and *Botrytis cinerea*. *Pseudomonas fluorescens* and *Botrytis cinerea* showed inhibition ranging from 3–10 mm and 2–4 mm, respectively, in the presence of 100 μL of active matrix of the film, which specifically inhibited hyphal growth. After incubation, the CaSS/CAR/GUG/CS/PPP/ChNP3 sample exhibited an 8 ± 0.34 inhibition zone against *Pseudomonas fluorescens*. Moreover, the maximum zone of inhibition of 4 ± 0.10 mm against *Botrytis cinerea*, and 10 ± 0.21 mm against *Pseudomonas fluorescens*, respectively, showed that increasing the ChNP concentration from 3 to 5% improved the inhibitory effect. Numerous active substances that are present in the film matrix have a variety of curative characteristics including antimicrobial effects. Previous research has shown that there is a direct correlation between the antimicrobial activity and the matrix concentration (%).[87]

Table SI.1 to 6 mentions the bioactive compounds which possessed antimicrobial characteristics, including O-cymene, β-caryophyllene, α-pinene, β-pinene, camphene, spathulenol, germacrene, myrcene, annonacin, and molvizarin. Additionally, the existence of β-caryophyllene contributes to its antibacterial and antimicrobial properties.[88] The CaSS/CAR/GUG film did not demonstrate any growth inhibition activity, as anticipated. On the other hand, the incorporation of PPP and ChNPs exhibited good antimicrobial efficacy against microorganisms such as *Pseudomonas fluorescens* and *Botrytis cinerea*. When ChNPs were present at concentrations of up to 5%, the inhibition activity slightly increased (Table 2). When 10% and 15% of chitosan nanoparticles were added to tara gum films, similar

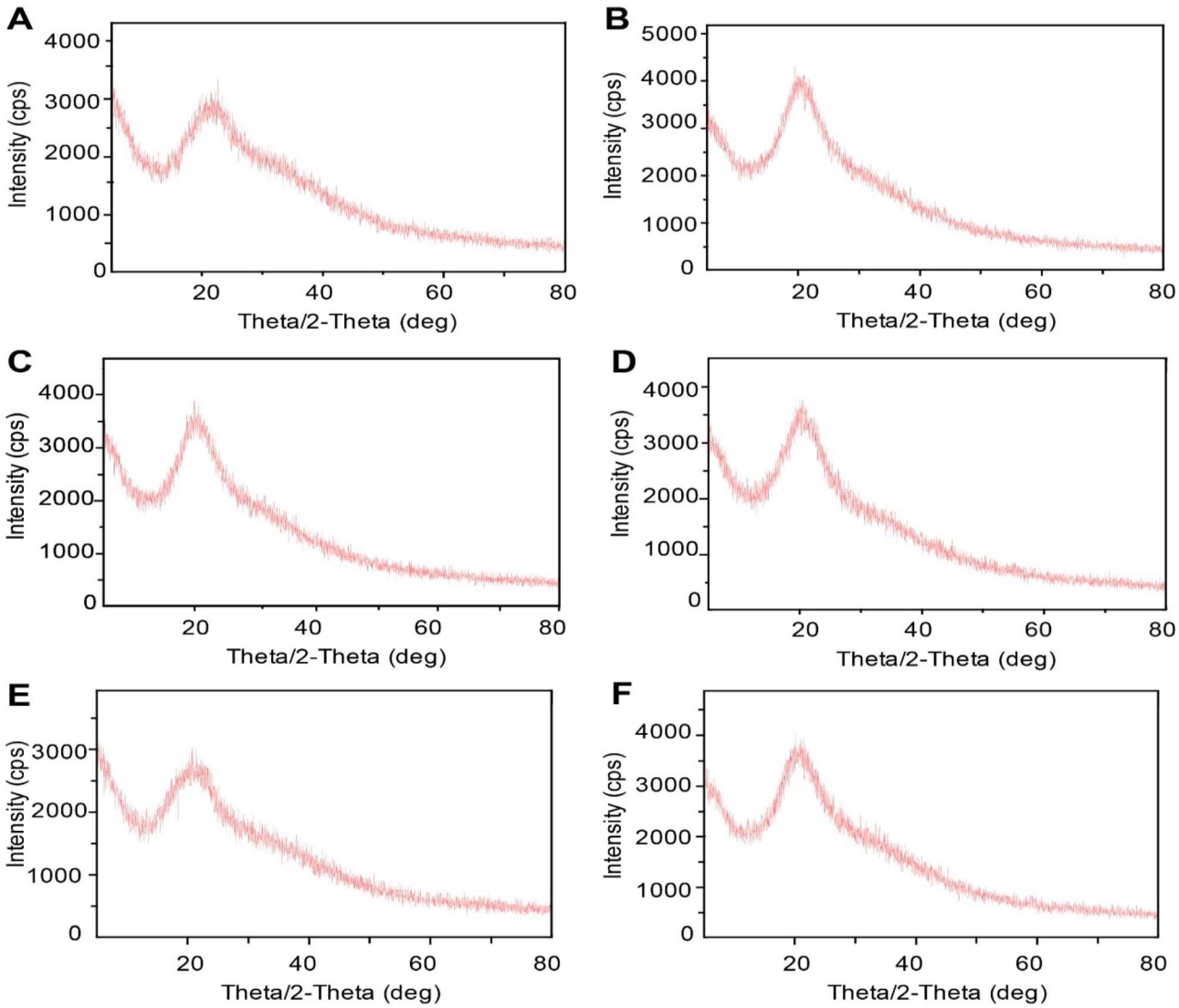

Fig. 4 XRD diffractograms of (A) CaSS/CAR/GUG; (B) CaSS/CAR/GUG/CS; (C) CaSS/CAR/GUG/CS/PPP; (D) CaSS/CAR/GUG/CS/PPP/ChNP1; (E) CaSS/CAR/GUG/CS/PPP/ChNP3; and (F) CaSS/CAR/GUG/CS/PPP/ChNP5 films.

Table 2 Diameter of the zone (mm) of film forming solution wells for inhibition of microbiological growth. The results are expressed as the mean of three different trials, with statistical significance ($p < 0.05$) and standard deviation determined according to one sample '*T*' test

Films	Diameter of the zone of inhibition (mm)	
	Pseudomonas fluorescence	*Botrytis cinerea*
CaSS/CAR/GUG	—	—
CaSS/CAR/GUG/CS	2 ± 0.23	—
CaSS/CAR/GUG/CS/PPP	5 ± 0.88	2 ± 0.98
CaSS/CAR/GUG/CS/PPP/ChNP1	7 ± 0.51	3 ± 0.20
CaSS/CAR/GUG/CS/PPP/ChNP3	8 ± 0.34	3 ± 0.44
CaSS/CAR/GUG/CS/PPP/ChNP5	10 ± 0.21	4 ± 0.10

antimicrobial activity was observed.[31] As *Pseudomonas fluorescens* and *Botrytis cinerea* have different cell wall structures, the ChNP loaded films demonstrated superior activity against this species. When PPP and polycationic ChNPs attach to the bacterial cell wall, they break the membrane, permitting intercellular compounds to pass through and cause cell death. Additionally, the PPP and ChNPs formed a barrier by interacting with the cell wall that limits the vital oxygen and nutrients, limiting the microorganism's development and metabolic processes.[31] Thus, adding CaSS, PPP and the ChNP loaded film to the postharvest preservation of litchi may decrease the rate of deterioration and increase the shelf life of the litchi.

3.2.8 Biodegradability test. The susceptibility of films to environmental degradation, usually by microorganisms, is assessed based on their biodegradability. Using processes involving biodeterioration, depolymerization, assimilation, and mineralization, the complex polymers undergo conversion to monomers.[89] Fig. 5 illustrates a picture of the films taken before and after the 20 day soil burial test. After 20 days, the CaSS/CAR/GUG films exhibited a weight loss of 61.29 ± 1.34%, reflecting the strong water-absorbing capacity of the hydrophilic starch molecules, which weakens intermolecular interactions in the film matrix and accelerates degradation. The weight loss slightly increased to 62.69 ± 2.98% ($p < 0.05$) upon the addition of CS and PPP. This was assigned to the strong connections between the polymer's molecules, which constrained the penetration of water molecules within the matrix of the film. Incorporating ChNPs promotes an accelerated rate of breakdown with smaller particles, with the highest reduction in weight of 73.54 ± 2.67% at 5% ChNP concentration.

The integrated nanoparticles may have contributed to biopolymer degradation through hydrolysis by exhibiting catalytic activity. However, previous research has reported that the incorporation of chitosan nanoparticles into tamarind kernel xyloglucan (XG) and jamun seed starch (JaSS) films similarly enhanced their biodegradability.[17] The ChNP loaded CaSS/CAR/GUG/CS/PPP nanocomposite films generally showed a short lifespan in the biological environment, indicating their potential for the development of biodegradable packaging films.

4 Shelf-life studies on the fresh litchi

Upon characterization of the developed films, the developed films were applied to fresh litchi to explore the practical applicability of the films. Different quality attributes were analysed at

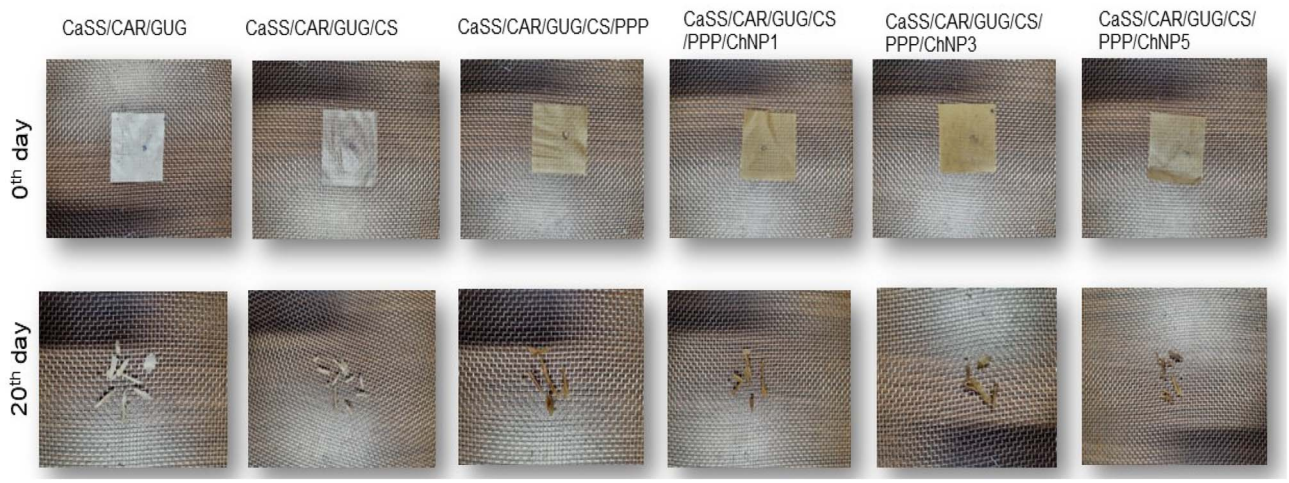

Fig. 5 Snapshot of the films before and after the soil burial test.

regular intervals under storage conditions of 27 ± 2 °C for five days to determine their effectiveness. These attributes included moisture content, weight loss percentage, pH, firmness, TSS, TA, TSS : TA ratio, percent of fresh litchi, colour, and sensory attributes. Fig. 6 illustrates the snapshots of litchi fruits with the developed films over different storage days. The variations in moisture content, color, and the percentage of fresh litchi were analyzed to evaluate microbial growth and discoloration, which are indicative of the fruit's end of shelf life during storage, as illustrated in Fig. 7 and 8. The discussion of each parameter has been given below.

4.1 Sensory evaluation

In conjunction with physicochemical assessment, sensory evaluation is essential for determining the overall acceptability and shelf life of litchi. Considering characteristics like taste, texture, aroma, freshness, colour, and overall acceptability provides substantial data on consumer preferences and product quality over time. Throughout the 0^{th} day of storage, the sensory characteristics of the litchi in every sample remained relatively stable at 27 ± 2 °C and 65 ± 5% RH.

The litchi samples packed in CaSS/CAR/GUG films exhibited overall acceptability scores up to the 2nd day, as shown in Fig. 7C. However, by the 3rd day, a noticeable decline in quality attributes, including freshness, colour, aroma, taste, and texture, was observed in CaSS/CAR/GUG film samples, resulting in sensory scores falling below the acceptable threshold. In contrast, litchis stored with the ChNP loaded CaSS/CAR/GUG/CS/PPP nanocomposite films maintained acceptable sensory attributes throughout the 5 days of storage period, with slight decreases observed by the 4th day. Panellists consistently preferred litchis packed in CaSS/CAR/GUG/CS/PPP/ChNP3 films within the sensory threshold level, indicating their preference for these samples over CaSS/CAR/GUG film samples.

Overall, in comparison to ChNP loaded CaSS/CAR/GUG/CS/PPP nanocomposite film samples, these results generally show that they had a longer shelf life and were more susceptible to sensory attributes.

The findings of the physicochemical analyses and the sensory evaluation show the efficacy of the produced films in prolonging the shelf life of litchi. By correlating sensory attributes with other quality parameters, a comprehensive assessment of litchi spoilage was achieved, providing deeper insight into its shelf- life dynamics.

4.2 Moisture content

To maintain their vibrancy and physiological function, litchis have moisture content of more than 80%. Litchi has limited shelf life caused by their high moisture content, which has a major effect on the litchi texture, colour, form, and weight. This may further impact the storage stability and shelf life of litchi. Thus, it is essential to monitor moisture content to assess the litchi's freshness.

Fig. 8A illustrates the moisture content of litchi stored at 27 ± 2 °C and 65 ± 5% RH. After two days, the moisture content of the litchi decreased significantly ($p < 0.05$) in the CaSS/CAR/GUG film (78.12 ± 0.09%) with a slight decrease in the films loaded with ChNPs of 1, 3, and 5% (80.94 ± 0.10%, 81.01 ± 0.10%, and 81.03 ± 0.06%, respectively). The 5th day of storage resulted in a moisture fall (75.14 ± 0.04%) in the CaSS/CAR/GUG film samples. In contrast, the 5% ChNP loaded CaSS/CAR/GUG/CS/PPP nanocomposite film showed a minimal amount of moisture decrease (80.08 ± 0.08% on the 5th day). The CaSS/CAR/GUG samples were eliminated on the 3rd day of storage because of softness and loss in texture, which was equivalent to a decrease in moisture content of more than 5%.

Nevertheless, as the moisture content decreases, it can lead to deterioration and the growth of microbes. However, CaSS/CAR/GUG/CS/PPP/ChNPs 1 to 5% nanocomposite films

Fig. 6 A comparison of the post-harvest quality of litchi stored for up to five days at 27 ± 2 °C and 65% RH.

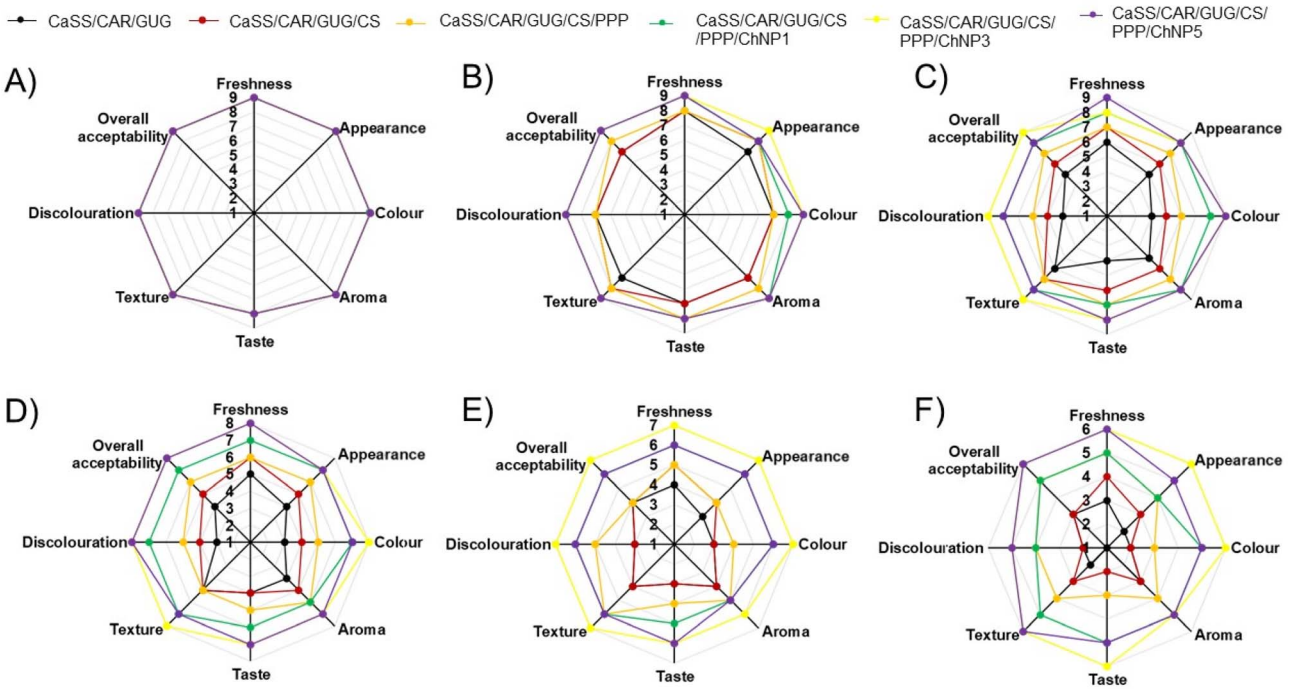

Fig. 7 The impact of the films on the sensory characteristics of litchis on the 0th day (A); 1st day (B); 2nd day (C); 3rd day (D); 4th day (E); and 5th day (F) (mean ± standard deviation of three replicates) stored for a period of 5 days at 27 ± 2 °C and 65 ± 5% RH.

maintain moisture content within the litchi and showed very little moisture loss throughout storage.

4.3 pH values

The acidity or alkalinity of food is indicated by its pH value. The pH value of litchis is a critical parameter influencing their quality, as it reflects enzymatic activity and biochemical processes, such as colour changes occurring during the storage period. In litchi, the pH typically falls within the slightly acidic range of 3.35 to 5.22, contributing to their flavour profile and microbial stability. Maintaining a stable pH is essential for preserving the quality and safety of litchi, impacting factors such as taste, texture, and microbial growth inhibition.

At 27 ± 2 °C with 65 ± 5% RH, the pH of litchi decreased during storage, as depicted in Fig. 8B. Initially, on the 0th day, all litchi samples exhibited similar pH values of 5.22 ± 0.020. However, by the 1st day of storage, a significant decrease in pH was observed, with CaSS/CAR/GUG samples showing pH values of 4.89 ± 0.015 and ChNP loaded CaSS/CAR/GUG/CS/PPP nanocomposite samples recording pH values of between 5.17 ± 0.010 to 5.18 ± 0.005. By the 5th day, the pH further decreased significantly to 4.35 ± 0.063 for CaSS/CAR/GUG samples and maintained the highest pH of 4.91 ± 0.010 for CaSS/CAR/GUG/CS/PPP/ChNP3 samples, with other films displaying the lowest pH values. This decline in pH over the storage period reflects microbial activity in the litchi, with CaSS/CAR/GUG samples exhibiting more pronounced acidity compared to other samples as discussed earlier.

Overall, the nanocomposite loaded films demonstrated superior efficiency in preserving pH levels compared to other samples. This finding suggests reduced microbial activity and minimal pH reduction in litchi, highlighting the role of bio-nanocomposite films in enhancing the shelf life of litchi. The observed differences in pH values underscore the importance of bio-nanocomposite films in maintaining the quality and safety of litchi during storage.

4.4 Firmness

Firmness is a crucial quality characteristic that customers take into account when assessing the maturity of a fruit. In this study, the firmness of all samples exhibited a general downward trend, indicating that the fruits become softer during storage (Fig. 8C).

The firmness of the litchi ranged from 9.23 ± 0.020 to 9.25 ± 0.005 N on the 0th day. The CaSS/CAR/GUG film showed a rapid drop of firmness to 6.73 ± 0.159 N on the 5th day and 3% ChNP loaded CaSS/CAR/GUG/CS/PPP nanocomposite films exhibited a higher firmness of 8.82 ± 0.058 N on the 5th day of storage. This decrease in firmness corresponds with the reduction in moisture content, weight loss, and microbial decay which contribute to shrinkage and skin damage.[81]

Previous studies have also reported a reduction in firmness in various fruits.[90] The reduction in fruit firmness is likely due to alterations in the cell wall structure caused by degrading enzymes such as polygalacturonase and breakdown of starch, cellulose, and hemicellulose.[91] Moreover, similar results have been reported in other studies, showing a decreasing trend in litchi firmness during storage.[4,12,13]

This decrease in firmness is a key indicator of the ripening process, reflecting the biochemical and physiological changes

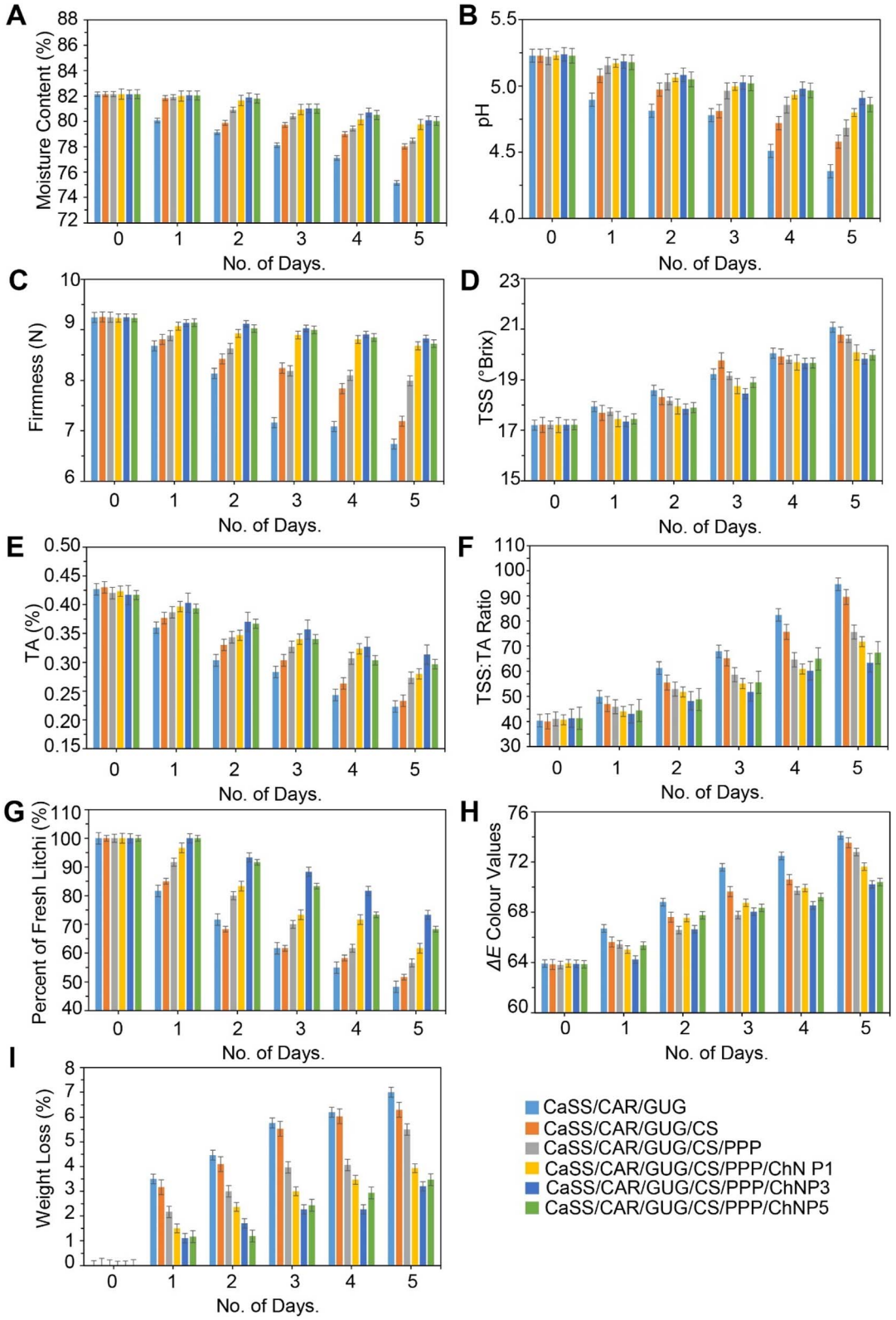

Fig. 8 (A) Moisture content; (B) pH values; (C) firmness; (D) total soluble solid content; (E) titratable acidity; (F) TSS : TA ratio; (G) percentage of fresh litchi; (H) Δ*E* colour values and (I) weight loss percentage at 27 ± 2 °C with 65 ± 5% RH for *Litchi chinensis*. The results are represented as the average of three distinct trials, and ANOVA and *Post hoc* tests (Duncan test) are used to establish the statistical significance and standard deviation.

occurring within the fruit. As the cell wall components break down and moisture content decreases, the fruit's texture softens, impacting its overall quality and consumer appeal. The firmness data, in conjunction with moisture content, weight loss and pH values highlight the importance of bio-nanocomposite films in maintaining fruit maturity and quality of litchi.

4.5 Total soluble solid (TSS)

The TSS content serves as a crucial indicator of litchi quality, directly influencing their maturity, flavour, freshness, taste, and moisture content. A higher TSS value is often associated with the onset of discoloration, indicating significant water loss. Therefore, close monitoring of TSS is essential for maintaining litchi quality.

Fig. 8D illustrates the changes in TSS content between different samples of litchi during the storage period. As the storage period progressed, TSS levels of litchi in all samples increased over the five day storage period. This is due to the fact that during physiological metabolism, nutrients like starch and cellulose in litchi fruits subsequently break down into monosaccharides and disaccharides.[92] The value of TSS in litchi of the CaSS/CAR/GUG film was significantly higher than that of the other films, with significant differences ($p < 0.05$) observed in the total soluble solid content. This is because the ChNP loaded CaSS/CAR/GUG/CS/PPP nanocomposite films decreased the respiration rate of litchi by restricting the movement of oxygen and other gases, thereby preventing the increase in TSS content.[93] Over five days of storage, the TSS of litchi with CaSS/CAR/GUG, CaSS/CAR/GUG/CS, and CaSS/CAR/GUG/CS/PPP films increased to 21.07 ± 0.025 °Brix, 20.77 ± 0.049 °Brix, and 20.61 ± 0.081 °Brix, respectively, while the CaSS/CAR/GUG/CS/PPP/ChNP3 composite film showed a minimal increase to 19.82 ± 0.26 °Brix. Similar results have been reported in other previous studies, revealing an increasing tendency in litchi TSS during storage.[12]

Fruit acidity is directly associated with TSS. During the fruit's storage, TSSs typically increase while fruit acidity typically decreases.[94] The increased TSS content with storage suggests the accumulation of sugars in litchi, potentially due to enzymatic activity or metabolic processes during storage. Overall, the observed bio-nanocomposite films maintaining TSS in litchi confirms the maintained sugar content during the fruit's storage.

4.6 Titratable acidity (TA)

Monitoring TA is crucial for assessing litchi quality during the storage period. Throughout storage, all samples showed a tendency toward decreasing TA, indicative of various metabolic processes. The variations in TA across different samples of litchi over 5 days are shown in Fig. 8E.

The respiration processes' utilisation of organic acids or metabolism of the litchi fruits causes the TA of all samples to decrease over the five days of storage.[95] The CaSS/CAR/GUG film had the lowest TA (0.22 ± 0.015%) at the end of storage. Litchi treated with CaSS/CAR/GUG/CS/PPP/ChNP 1, 3, and 5% nanocomposite films preserved their TA values better compared to the CaSS/CAR/GUG film throughout 5 days of the storage period. This could be an outcome of the nanocomposite film's tendency to decrease the microenvironment oxygen content, which delays the litchi's rate of respiration during storage and lowers their titratable acid absorption.[92] Specifically, over five days of storage, the TA value (0.31 ± 0.015%) of the litchi fruits treated with CaSS/CAR/GUG/CS/PPP/ChNP3 was statistically greater ($p < 0.05$) than that of other films. This was mainly due to the CaSS/CAR/GUG/CS/PPP/ChNP3 nanocomposite films exhibiting superior barrier properties.

The decreasing TA content in litchi during storage is due to the increase in the TSS/TA ratio, resulting from increasing TSS levels and decreasing TA values throughout the storage period. Similar findings from previous studies have been published, showing a tendency for litchi TA to decrease over storage.[13]

4.7 TSS : TA ratio

In fresh produce, flavor and taste are determined by the interplay of acidity and TSS, which change notably over the storage period. The TSS : TA ratio is a crucial factor affecting both the fruit's taste and consumer perception of its overall quality. Throughout storage, the TSS : TA ratio increased steadily in all litchi samples, and Fig. 8F displays the differences in TSS : TA ratios between different litchi samples over the 5 day storage period.

At the 0^{th} day, the TSS : TA ratio was between 40.05 ± 0.556 to 41.33 ± 0.598 for all litchi samples. During the 5th day of storage, the CaSS/CAR/GUG film exhibited the highest TSS : TA ratio (94.65 ± 6.404), while CaSS/CAR/GUG/CS/PPP/ChNP3 nanocomposite films had the lowest (63.35 ± 3.042) ratio.

At the 0^{th} day, the TSS : TA ratio was between 40.05 ± 0.556 to 41.33 ± 0.598 for all litchi samples. During the 5th day of storage, the CaSS/CAR/GUG film exhibited the highest TSS : TA ratio (94.65 ± 6.404), while CaSS/CAR/GUG/CS/PPP/ChNP3 nanocomposite films had the lowest (63.35 ± 3.042) ratio. These findings are consistent with the reported increase in the TSS : TA ratio in the litchi storage period.[96] A correlation was observed between the fresh produce's respiration activity during storage and an increase in the TSS : TA ratio. A higher TSS : TA ratio was enhanced by high TSS levels and low TA.

Overall, all litchi samples exhibited an increase in the TSS : TA ratio during the storage period. This increase in the TSS : TA ratio confirms the increasing sugar content in litchi, contributing to their enhanced maturity. These results highlight the importance of bio-nanocomposite films for maintaining the TSS : TA ratio to assess the quality of litchi.

4.8 Percent of fresh litchi

The percentage of fresh litchi samples over a 5 day storage period is shown in Fig. 8G. The percentage of fresh litchi was consistently higher in CaSS/CAR/GUG/CS/PPP 1, 3, and 5% nanocomposite films over the storage period compared to the CaSS/CAR/GUG, CaSS/CAR/GUG/CS, and CaSS/CAR/GUG/CS/PPP films. On the 5th day of storage, the CaSS/CAR/GUG, CaSS/CAR/GUG/CS, and CaSS/CAR/GUG/CS/PPP films exhibited fresh litchi with a discoloration of 48.33 ± 2.88%, 51.66 ± 2.88%, and 56.66 ± 2.88%, respectively. An illustration of the greater percentage of freshness in the CaSS/CAR/GUG/CS/PPP/

ChNP 1, 3, and 5% films on the 5th day revealed 61.66 ± 2.88%, 73.33 ± 2.88%, and 68.33 ± 2.88% of fresh litchi. In contrast, the CaSS/CAR/GUG film on the 5th day showed 48.33 ± 2.88% freshness of litchi and the CaSS/CAR/GUG/CS/PPP/ChNP3 film had the maximum level of freshness. The litchi freshness continued to fall within the acceptable limits, possibly due to the antimicrobial properties of the films. These results show that, in comparison to other films, the freshness of litchi was maintained in ChNP loaded bio-nanocomposite films.

4.9 Colour values

Colour assessment evaluates changes in the appearance of litchi during the storage period. Colour is a crucial parameter for assessing the freshness and quality of litchi, as changes in colour can indicate physiological changes, enzymatic activity, and deterioration during storage. As the litchi pericarp matures, environmental variables have an impact on its colour. The litchi colour (ΔE) of those packaged in films after up to five days of storage are displayed in Fig. 8H.

All litchi samples had a trend towards increasing ΔE colour values throughout the storage time. Comparing the ΔE values of the various litchi samples, the CaSS/CAR/GUG film had the greatest values. The findings indicated that enhanced enzymatic browning during storage caused ΔE values to considerably increase ($p < 0.05$) in all samples.[12] The discolouration of the pericarp and surface browning cause colour changes during storage. The litchi packed in films loaded with ChNPs showed slower discolouration compared to the other samples. This could be because of the compactness of the film, which acts as an interface for moisture loss. Similar findings from previous studies have been published, showing the tendency for litchi ΔE values during storage.[13]

4.10 Weight loss percentage

Fruit browning and spoilage are the main causes of weight loss, which is a common characteristic of horticulture crops during storage.[93] Fig. 8I illustrates that the weight loss of the litchi fruits significantly increased ($p < 0.05$) in different samples over the storage period.

Weight loss is increased due to respiration of the fruit, CO_2 transfer, and variations in vapour pressure that cause the litchis to lose moisture into their surroundings.[12] The CaSS/CAR/GUG (7.00 ± 0.10%), CaSS/CAR/GUG/CS (6.30 ± 0.30%), and CaSS/CAR/GUG/GUG/CS/PPP film samples (5.50 ± 0.26%) had the greatest weight loss on the end of the storage day. In contrast, the CaSS/CAR/GUG/CS/PPP/ChNP3 film had the lowest percentage of weight loss (3.20 ± 0.10%) on the 5th day. Previous studies have also revealed a tendency for litchi weight loss to increase over time.[12,13] While the ChNP enriched CaSS/CAR/GUG/CS/PPP films restricted water loss *via* a moisture impermeable layer, they maintained sufficient moisture to avoid significant weight loss in the litchis.[10] As fruits and vegetables have a high-water content, it is essential to avoid water loss to maintain postharvest quality.[4]

Overall, findings suggest that the ChNP loaded CaSS/CAR/GUG/CS/PPP bio-nanocomposite films effectively preserve the freshness, safety, and overall quality of litchi by controlling discolouration and water loss, and minimizing deterioration during storage. By reducing litchi moisture content, firmness and pH, the bio-nanocomposite films contribute to extending shelf life and enhancing freshness.

Thus, storing litchi with CaSS/CAR/GUG/CS/PPP/ChNP3 at 27 ± 2 °C and 65 ± 5% RH extended the shelf life to 5 days, maintaining freshness and quality attributes. This study highlights the potential of bio-nanocomposite films in enhancing litchi quality and extending shelf life, offering promising implications for the food preservation industry.

5 Conclusions

This study developed biodegradable bio-nanocomposite films based on custard apple seed starch (CaSS) reinforced with chitosan nanoparticles (ChNPs), pomegranate peel powder (PPP), corn starch (CS), carrageenan (CAR), and guar gum (GUG). Furthermore, the structural, physicochemical, mechanical, and barrier characteristics of the films were systematically assessed through FTIR, XRD, and GC-MS analyses. The results demonstrated strong synergistic interactions among CaSS, CAR, GUG, CS, PPP, and ChNPs, leading to significant improvements in rheological behavior, mechanical strength, and water vapor barrier performance. Moreover, utilization of CaSS derived from custard apple seed waste highlights the sustainability potential of the films through waste valorization, diversification of renewable raw materials, and value addition. Application of the optimized CaSS/CAR/GUG/CS/PPP/ChNPs 3% film effectively extended the shelf life of litchi by approximately 3 ± 1 day at 27 ± 2 °C and 65 ± 5% RH, while maintaining fruit quality and sensory attributes. Despite these promising outcomes, further investigation is necessary to overcome limitations including high water solubility, insufficient long term stability data, lack of nanoparticle migration studies, and role of individual component effects. Future research should focus on enhancing moisture resistance, evaluating food safety and scalability, and extending the application of these bio-nanocomposite films to other fresh produce and industrial packaging systems.

Author contributions

Sachin P. Shinde: conceptualization, methodology, supervision, visualization, formal analysis, investigation, data curation, writing – original draft. Swapnali S. Bhole: supervision, visualization, formal analysis, review & editing. Namita S. Patil: formal analysis, review & editing. Gurunath V. Mote: supervision, validation, review & editing. Vikramsinh M. Ingale: formal analysis, review & editing.

Conflicts of interest

The authors declare no conflict of interest.

Data availability

All data supporting the findings of this study are available within the article and its supplementary information (SI). Additional datasets generated or analysed during the current study are available from the corresponding author on reasonable request, in accordance with the *Royal Society of Chemistry's* data availability policy. Supplementary information is available. See DOI: https://doi.org/10.1039/d5fb00721f.

Acknowledgements

This research did not receive any specific grant from funding agencies in the public, commercial, or not-for-profit sectors. We acknowledge Dr Sanjay D. Patil, Chancellor, DYP-ATU, Talsande and Dr Anilkumar Gupta, Vice Chancellor, DYP- ATU, Talsande for extending the facilities and support for this work.

References

1 V. Nath, G. Kumar, S. D. Pandey and A. K. Gupta, *Acta Hortic.*, 2018, **1211**, 153–160.
2 A. Fan, C. Wan, H. Liu, X. Xiong, Y. Nong, İ. Kahramanoğlu, R. Yang and L. Zeng, *Food Chem.:X*, 2023, **19**, 100796–100807.
3 X. Yu, J. Chen, J. Zhong, W. Deng, Z. Zhang, Y. Wu and Q. Zheng, *Food Control*, 2023, **154**, 110019.
4 M. M. Molla, E. Rahman, A. Khatun, M. F. Islam, M. Z. Uddin, M. A. Ullah, M. G. Saha and M. Miaruddin, *Am. J. Food Technol.*, 2017, **12**, 322–331.
5 D. Khodaei, Z. Hamidi-Esfahani and E. Rahmati, *NFS J.*, 2021, **23**, 17–23.
6 L. K. Vora, A. D. Gholap, K. Jetha, R. R. S. Thakur, H. K. Solanki and V. P. Chavda, *Artificial Intelligence in Pharmaceutical Technology and Drug Delivery Design*, 2023, vol. 15.
7 M. Guo, Z. Li, J. Liu, J. Yu, J. Ren and Q. Li, *Chem. Eng. J.*, 2024, **502**, 158092.
8 L. Zhang, W. He, Y. Ping, W. Wang, P. Hu, B. Li, W. Zhu, J. Sun, Y. Ji and J. Wang, *Chem. Eng. J.*, 2024, **491**, 152116.
9 F. Xie, X. Feng, Z. Wang, D. Zhang, Q. Chen, Z. He, S. He, X. Wang, Y. Wu and J. Cai, *Chem. Eng. J.*, 2024, **496**, 154113–154128.
10 T. Sharma, G. Kaur, A. Singh and P. Singh, *J. Food Meas. Charact.*, 2023, **17**, 5550–5568.
11 A. Vaidya, N. Solanke and K. Gaware, *Int. J. Sci. Eng. Technol.*, 2016, **5**, 205–209.
12 T. Sharma, G. Kaur, A. Singh, V. Kumar and B. N. Dar, *Sci. Hortic.*, 2024, **332**, 113239–113252.
13 F. Liang, C. Liu, J. Geng, N. Chen, W. Lai, H. Mo and K. Liu, *Carbohydr. Polym.*, 2024, **333**, 121968–121983.
14 R. Santhosh and P. Sarkar, *Int. J. Biol. Macromol.*, 2024, **260**, 129625.
15 W. Ma, C. H. Tang, X. Q. Yang and S. W. Yin, *Food Hydrocolloids*, 2013, **31**, 237–247.
16 A. Nawab, F. Alam, M. A. Haq, Z. Lutfi and A. Hasnain, *Int. J. Biol. Macromol.*, 2017, **98**, 869–876.
17 R. Santhosh and P. Sarkar, *Food Hydrocolloids*, 2022, **133**, 107917.
18 T. L. Cao and K. Bin Song, *Food Hydrocolloids*, 2019, **97**, 105198.
19 A. Tamang, S. Subba and S. Chhetri, *Pharma Innov. J.*, 2021, **10**, 609–613.
20 N. Rais, D. Chandran, A. Dey, T. Sarkar, S. Dhumal and S. Kumar, *Processes*, 2022, **10**, 1–20.
21 H. Gangurde, A. Prof and M. Raut, *Int. J. Res. Publ. Rev.*, 2023, **4**, 1321–1326.
22 C. Shanbhag, R. Shenoy, P. Shetty, M. Srinivasulu and R. Nayak, *J. Food Sci. Technol.*, 2023, **60**, 2858–2867.
23 S. K. H. Shah Bukhary, F. K. Choudhary, D. N. Iqbal, Z. Ali, A. Sadiqa, S. Latif, K. M. Al-Ahmary, S. Basheer, I. Ali and M. Ahmed, *RSC Adv.*, 2024, **14**, 19349–19361.
24 T. Dhilipkumar, A. M. Sadeq, P. Karuppusamy, K. V. Shankar, A. P. Murali, A. A. Darem, K. Selvakumar and J. Giri, *Eur. Food Res. Technol.*, 2025, **251**, 3151–3173.
25 Y. Ali, J. Ahmed, N. Hiremath, R. Auras and A. Joseph, *Food Hydrocolloids*, 2017, **62**, 191–202.
26 Y. Bai, T. Qiu, B. Chen, C. Shen, C. Yu, Z. Luo, J. Zhang, W. Xu, Z. Deng, J. Xu and H. Zhang, *Carbohydr. Polym.*, 2023, **312**, 120693.
27 N. Basavegowda and K.-H. Baek, *Polymers*, 2021, **13**, 4198.
28 N. Vahedikia, F. Garavand, B. Tajeddin, I. Cacciotti, S. M. Jafari, T. Omidi and Z. Zahedi, *Colloids Surf., B*, 2019, **177**, 25–32.
29 P. R. Chang, R. Jian, J. Yu and X. Ma, *Food Chem.*, 2010, **120**, 736–740.
30 C. Geng, X. Liu, J. Ma, H. Ban, H. Bian and G. Huang, *Carbohydr. Polym.*, 2023, **306**, 120612.
31 J. Antoniou, F. Liu, H. Majeed and F. Zhong, *Food Hydrocolloids*, 2015, **44**, 309–319.
32 J. Antoniou, F. Liu, H. Majeed, H. J. Qazi and F. Zhong, *Carbohydr. Polym.*, 2014, **111**, 359–365.
33 C. Chandra Mohan, K. R. Rakhavan, K. Radha Krishnan, S. Babuskin, K. Sudharsan, P. Azhagu Saravana Babu and M. Sukumar, *LWT–Food Sci. Technol.*, 2016, **72**, 239–250.
34 K. A. Iyer, L. Zhang and J. M. Torkelson, *ACS Sustain. Chem. Eng.*, 2016, **4**, 881–889.
35 K. Harini, C. Chandra Mohan, K. Ramya, S. Karthikeyan and M. Sukumar, *Carbohydr. Polym.*, 2018, **184**, 231–242.
36 Z. A. N. Hanani, F. C. Yee and M. A. R. Nor-Khaizura, *Food Hydrocolloids*, 2019, **89**, 253–259.
37 S. F. Hosseini, M. Rezaei, M. Zandi and F. Farahmandghavi, *Food Hydrocolloids*, 2015, **44**, 172–182.
38 K. Helrich, *Off. Methods Anal. Assoc. Off. Anal. Chem.*, 1990, **2**, 425–497.
39 K. Rengsutthi and S. Charoenrein, *Lwt*, 2011, **44**, 1309–1313.
40 S. Lu, T. T. Cik, C. yi Lii, P. Lai and H. H. Chen, *Lwt*, 2013, **54**, 224–228.
41 P. Suraj, M. Shantanu, S. P. Patil, S. R. Chaudhari and R. S. Matche, *ACS Sustain. Chem. Eng.*, 2023, **11**, 8764–8773.
42 S. P. Shinde, S. R. Chaudhari and R. S. Matche, *Postharvest Biol. Technol.*, 2023, **204**, 112475.
43 T. Ghosh, K. Mondal, B. S. Giri and V. Katiyar, *Food Chem.*, 2021, **360**, 130048–130059.

44 Y. Y. Qin, Z. H. Zhang, L. Li, M. L. Yuan, J. Fan and T. R. Zhao, *J. Food Sci. Technol.*, 2015, **52**, 1471–1479.
45 U. Siripatrawan and B. R. Harte, *Food Hydrocolloids*, 2010, **24**, 770–775.
46 Y. Asahi, J. Miura, T. Tsuda, S. Kuwabata, K. Tsunashima, Y. Noiri, T. Sakata, S. Ebisu and M. Hayashi, *AMB Express*, 2015, **5**, 1–9.
47 D. Nath, S. Ravichandran, J. Ahmed and P. Sarkar, *J. Food Process Eng.*, 2022, **45**, 1–8.
48 S. Mathew, S. S, J. Mathew and E. K. Radhakrishnan, *Food Packag. Shelf Life*, 2019, **19**, 155–166.
49 M. Przeor and E. Flaczyk, *Indian J. Tradit. Knowl.*, 2016, **15**(2), 237–244.
50 B. K. Baidya and S. Chakrabarty, *Int. J. Curr. Microbiol. Appl. Sci.*, 2020, **9**, 664–674.
51 S. P. Shinde, G. R. Hon, P. Suraj, S. R. Chaudhari and R. S. Matche, *ACS Food Sci. Technol.*, 2024, **4**, 2134–2145.
52 S. P. Shinde, D. T. Wagai, G. R. Hon, P. Suraj, S. R. Chaudhari and R. S. Matche, *ACS Food Sci. Technol.*, 2024, **4**, 3047–3058.
53 P. Gunness, O. Kravchuk, S. M. Nottingham, B. R. D'Arcy and M. J. Gidley, *Postharvest Biol. Technol.*, 2009, **52**, 164–172.
54 S. P. Shinde, S. Payyadakkath, A. Biswas, G. R. Hon, R. S. Matche and S. R. Chaudhari, *J. Food Compos. Anal.*, 2025, **142**, 107526.
55 P. Kwanhong, O. Suwanchom, S. Srithanyarat, K. Songchan and J. Singto, *Acta Hortic.*, 2018, **1210**, 87–94.
56 M. Ghasemlou, N. Aliheidari, R. Fahmi, S. Shojaee-Aliabadi, B. Keshavarz, M. J. Cran and R. Khaksar, *Carbohydr. Polym.*, 2013, **98**, 1117–1126.
57 B. Wang, Y. Dong, Y. Fang, W. Gao, X. Kang, P. Liu, S. Yan, B. Cui and A. M. Abd El-Aty, *Food Chem.*, 2022, **368**, 130804–130811.
58 E. Sabella, A. Aprile, A. Genga, T. Siciliano, E. Nutricati, F. Nicolì, M. Vergine, C. Negro, L. De Bellis and A. Luvisi, *Sci. Rep.*, 2019, **9**, 1–12.
59 M. R. De Moura, F. A. Aouada, R. J. Avena-Bustillos, T. H. McHugh, J. M. Krochta and L. H. C. Mattoso, *J. Food Eng.*, 2009, **92**, 448–453.
60 A. R. Dudhani and S. L. Kosaraju, *Carbohydr. Polym.*, 2010, **81**, 243–251.
61 M. Karimi, P. Avci, M. Ahi, T. Gazori, M. R. Hamblin, H. Naderi-Manesh and J. Nanopharmaceutics, *Drug Delivery*, 2014, **1**, 266–278.
62 P. Calvo, C. Remuñán-López, J. L. Vila-Jato and M. J. Alonso, *J. Appl. Polym. Sci.*, 1997, **63**, 125–132.
63 S. K. Debnath, S. Saisivam, M. Debanth and A. Omri, *PLoS One*, 2018, **13**, e0190976.
64 S. Shankar and J. W. Rhim, *Food Hydrocolloids*, 2018, **82**, 116–123.
65 F. Jin and Y. Li, *Catal. Today*, 2009, **145**, 101–107.
66 H. Cui, D. Surendhiran, C. Li and L. Lin, *Food Packag. Shelf Life*, 2020, **24**, 100511.
67 X. Zhang, Y. Liu, H. Yong, Y. Qin, J. Liu and J. Liu, *Food Hydrocolloids*, 2019, **94**, 80–92.
68 N. H. Marei, E. A. El-Samie, T. Salah, G. R. Saad and A. H. M. Elwahy, *Int. J. Biol. Macromol.*, 2016, **82**, 871–877.
69 M. Anand, P. Sathyapriya, M. Maruthupandy and A. H. Beevi, *Front. Lab. Med.*, 2018, **2**, 72–78.
70 A. Babaei-Ghazvini, I. Shahabi-Ghahfarrokhi and V. Goudarzi, *Food Packag. Shelf Life*, 2018, **16**, 103–111.
71 A. H. Ghadimi, S. Amiri and M. Radi, *Int. J. Biol. Macromol.*, 2024, **256**, 128456.
72 L. Zhang, D. Yu, Y. Gu, Y. Xu, Q. Jiang, F. Yang, J. M. Regenstein, D. Yu and W. Xia, *Food Hydrocolloids*, 2024, **150**, 109667.
73 B. Biduski, F. T. da Silva, W. M. da Silva, S. L. de M. El Halal, V. Z. Pinto, A. R. G. Dias and E. da R. Zavareze, *Food Chem.*, 2017, **214**, 53–60.
74 M. Mujtaba, B. Koc, A. M. Salaberria, S. Ilk, D. Cansaran-Duman, L. Akyuz, Y. S. Cakmak, M. Kaya, K. M. Khawar, J. Labidi and S. Boufi, *Int. J. Biol. Macromol.*, 2019, **133**, 663–673.
75 P. C. Martins, J. M. Latorres and V. G. Martins, *LWT–Food Sci. Technol.*, 2022, **156**, 113041–113051.
76 J. W. Rhim, S. I. Hong, H. M. Park and P. K. W. Ng, *J. Agric. Food Chem.*, 2006, **54**, 5814–5822.
77 R. Yekta, L. Mirmoghtadaie, H. Hosseini, S. Norouzbeigi, S. M. Hosseini and S. Shojaee-Aliabadi, *Int. J. Biol. Macromol.*, 2020, **158**, 327–337.
78 R. Kumar, G. Ghoshal and M. Goyal, *Lwt*, 2021, **145**, 111380.
79 C. Wu, Y. Li, Y. Du, L. Wang, C. Tong, Y. Hu, J. Pang and Z. Yan, *Food Hydrocolloids*, 2019, **89**, 682–690.
80 L. Li, Y. Hong, Z. Gu, L. Cheng, Z. Li and C. Li, *Food Hydrocolloids*, 2018, **77**, 825–833.
81 L. Cao, T. Ge, F. Meng, S. Xu, J. Li and L. Wang, *Food Hydrocolloids*, 2020, **98**, 105251–105260.
82 T. Ghosh and V. Katiyar, *Int. J. Biol. Macromol.*, 2022, **211**, 116–127.
83 R. Shahvalizadeh, R. Ahmadi, I. Davandeh, A. Pezeshki, S. A. Seyed Moslemi, S. Karimi, M. Rahimi, H. Hamishehkar and M. Mohammadi, *Food Chem.*, 2021, **354**, 129492.
84 N. L. Santos, R. C. Braga, M. S. R. Bastos, P. L. R. Cunha, F. R. S. Mendes, A. M. M. T. Galvão, G. S. Bezerra and A. A. C. Passos, *Int. J. Biol. Macromol.*, 2019, **132**, 1163–1175.
85 Z. Liu, C. Wang, X. Liao and Q. Shen, *Food Hydrocolloids*, 2020, **108**, 106081.
86 C. He, Y. Liu, H. Liu, X. Zheng, G. Shen and J. Feng, *Food Res. Int.*, 2020, **130**, 1–9.
87 N. R. Bhalodia, P. B. Nariya and V. J. Shukla, *Int. J. PharmTech Res.*, 2011, **3**, 160–168.
88 C.-L. Moo, S.-K. Yang, M.-A. Osman, M. H. Yuswan, J.-Y. Loh, W.-M. Lim, L. I. M. SWEE-HUA-ERIN and K.-S. Lai, *Pol. J. Microbiol.*, 2020, **69**, 49–54.
89 B. Singhal, S. Kumar, S. Mehtab, U. Aggarwal, V. Kumar, M. Umesh and P. Chakraborty, *Case Stud. Chem. Environ. Eng.*, 2024, **9**, 100640–100658.
90 N. Boudhrioua, C. Michon, G. Cuvelier and C. Bonazzi, *J. Food Eng.*, 2002, **55**, 115–121.
91 V. E. Nambi, K. Thangavel, K. A. Rajeswari, A. Manickavasagan and V. Geetha, *Postharvest Biol. Technol.*, 2016, **117**, 152–160.

92 F. Ebrahimi and S. Rastegar, *Sci. Hortic.*, 2020, **265**, 109258–109267.
93 W. Zhou, Y. He, F. Liu, L. Liao, X. Huang, R. Li, Y. Zou, L. Zhou, L. Zou, Y. Liu, R. Ruan and J. Li, *Carbohydr. Polym.*, 2021, **256**, 117579–117588.
94 M. S. Padda, C. V. T. do Amarante, R. M. Garcia, D. C. Slaughter and E. J. Mitcham, *Postharvest Biol. Technol.*, 2011, **62**, 267–274.
95 L. Dong, Q. Jiao, J. Gao, X. Luo, Y. Song, T. Li, C. Huan, M. Huang, G. Ren, Q. Shen, L. Fu, H. Xie and Z. Luo, *LWT—Food Sci. Technol.*, 2023, **182**, 114918–114927.
96 R. R. Mphahlele, O. J. Caleb and M. E. K. Ngcobo, *Heliyon*, 2020, **6**, e03229–e03239.